Selection and optimization of the seeding procedure prior to the synthesis of Pd-based membranes

Earl Mc Donald

A thesis submitted in partial fulfilment of the requirements for the degree of Master Philisophiae in the Department of Physics, University of the Western Cape.

Supervisor:

Dr S. Halindintwali

Co-supervisors:

Prof. B.J. Bladergroen

Prof. B. Julies

UNIVERSITY of the
WESTERN CAPE

March 2014

Abstract:

Pd based membranes are known for their incredible selectivity towards H_2. In order for Pd membranes to display high H_2 selectivity, a defect free layer of Pd needs to be deposited onto a support. Although various fabrication techniques do exist, many researchers have attempted to produce defect free Pd-based films, using electroless plating. The first step in the preparation technique involves “seeding” of the support structure. Even though these seeds, if well distributed and anchored to the support, are crucial in order to obtain the defect free Pd layer, they hardly ever received attention from the science community. This thesis reports findings on various seeding methods as well as the resulting microstructures of the Pd films formed as a result of the type of seeding method employed. Finally the quality of the membranes using the most promising seeding technique was determined by subjecting the membranes to permeance tests with N_2 at both high and low temperatures as well as with H_2 at high temperatures.

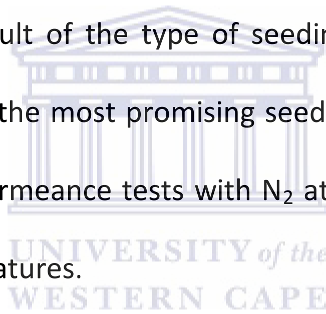

Declaration

I declare that *Selection and optimization of the seeding procedure prior to the synthesis of Pd-based membranes* is my own work, that it has not been submitted for any degree or examination in any other university, and that all sources I have used or quoted have been indicated and acknowledged by complete references.

Earl Mc Donald **February 2014**

Signature: ___________________

UNIVERSITY of the
WESTERN CAPE

Dedication

First and foremost I would like to give thanks to God Almighty for giving me the capability to have completed my masters. I would also like to thank him for watching over me and carrying me thus far, as it is only by his grace that I was able to get to this point in my life. I dedicate the work in my thesis to all the people in my life that have fully supported me and helped me to achieve my goals. To my parents Eric and Kathleen thanks for always caring and loving me. The guidance and support that you have given me is invaluable. To my sisters and the rest of my immediate family thanks for always believing in me and praying for me. Finally to my girlfriend Lezanne, thanks for all your love, support and encouragement.

UNIVERSITY of the
WESTERN CAPE

Acknowledgements

- Thanks to all my supervisors for all the expertise and guidance provided during my research
- I would like to thank everybody involved in the National Nanoscience Postgraduate Teaching and Training Programme (NNPTTP) for affording me the opportunity to be part of the masters programme
- Thanks to the DST for financially supporting the programme and the students.
- I would like to thank the South African Institute for Advanced Materials Chemistry (SAIAMC) for the provision and financial support of the research involved in this thesis
- To the Electron Microscope Unit (EMU) at the University of the Western Cape (UWC), thanks for all the expertise in the field of microscopy and the provision of the technical equipment.

Table of Contents

Chapter 1: Introduction 1

1.1 Hydrogen Production 1

1.2 Gas Separation Technology 3

1.3 Current problems associated with Pd based membrane 5

Chapter 2: Literature Review 8

2.1 Support Selection 8

2.1.1 Introduction 8

2.1.2 Types of Pd membrane supports 9

2.1.3 Characteristics of various supports 13

2.2 Introduction to Pd Membrane Fabrication 14

2.2.1 Chemical Vapour Deposition technique 14

2.2.2 Physical Vapour Deposition technique 15

2.2.3 Electroplating technique 16

2.2.4 Electroless Plating technique 16

2.3 Seeding 17

2.3.1 Introduction 17

2.3.2 Impact of seeding on plating 18

2.4 Seeding Methods 22

2.4.1 $SnCl_2$-$PdCl_2$ based Methods 22

2.4.2 Drawbacks of the $SnCl_2$-$PdCl_2$ based seeding method 24

2.4.3 Modified Seeding Methods 25

2.5 Surface Functionalisation 26

2.6 Permeance study of the palladium coated supports 27

2.7 Aims and objectives 28

2.8 Conclusion and Thesis Outline 28

2.8.1 Conclusion 28

2.8.2 Thesis Outline 29

Chapter 3: Experimental Methods 30

3.1 Materials and chemicals 30

3.2 The cleaning procedure of the supports 31

3.3 Seeding 32

3.3.1 Seeding Method 1 32

UNIVERSITY of the
WESTERN CAPE

3.3.2 Seeding Method 2 33
3.3.3 Seeding Method 3 34
3.3.4 Pre-seeding treatment 35
3.4 Plating 36
Chapter 4: Characterisation Techniques 39
4.1 Scanning Electron Microscopy 39
4.1.1 Introduction to Scanning Electron Microscopy 39
4.1.2 Components of the SEM and their functions 39
4.1.3 Image formation in SEM 43
4.1.4 Sample preparation for SEM characterisation 46
4.2 Transmission Electron Microscopy 46
4.2.1 Introduction to Transmission Electron Microscopy 46
4.2.2 Components of the TEM and their functions 47
4.2.3 Contrast mechanisms and image formation in TEM 50
4.2.4 Sample preparation for TEM characterisation 51
4.2.5 Electron Diffraction 51
4.2.6 Scanning Transmission Electron Microscopy 54
4.2.7 Energy Dispersive Spectroscopy 55
4.3 Permeance Testing 56
4.3.1 H_2 permeation through Pd membranes 56
4.3.2 Gas permeation tests 59
Chapter 5: Results and Discussion 61
5.1 SEM Analysis on seeded supports 61
5.2 TEM Analysis on seeded supports 69
5.3 Discussion of the results on seeded supports 74
5.4 SEM Analysis on plated supports 75
5.5 Discussion of the results on the plated supports 78
5.6 Permeance results and discussion on electroless plated samples 80
Chapter 6: Conclusion and Recommendations 87
6.1 Conclusion 87
6.2 Suggestions 88
References: 89

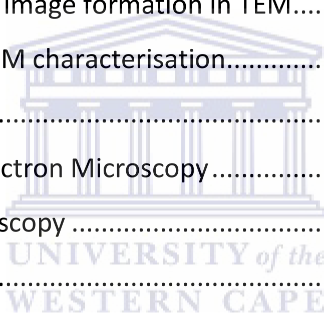
UNIVERSITY of the
WESTERN CAPE

List of figures:

Figure 1.1: Annual global H_2 production using various industrial techniques [1]................................. 1
Figure 1.2: Comparison of H_2 solubility for various metals at a pressure of 1 atm [1]. 4

Figure 2.1: Comparison between the deposition rates on seeded and clean supports [7]................. 19
Figure 2.2: illustration of film formation during plating 20
Figure 2.3: Schematic of the steps followed during the sensitisation- activation cycle 22
Figure 2.4: Schematic representation for Pd attachment to alumina support [16] 23
Figure 2.5: Schematic representation for Pd attachment to APTES attached to the support............. 26

Figure 3.1: Schematic of the procedure for seeding method 1 33
Figure 3.2: Schematic of the procedure for seeding method 2 34
Figure 3.3: Schematic of the procedure for seeding method 3 35
Figure 3.4: Schematic of the procedure for pre-seeding treatment 36
Figure 3.5: Schematic of the plating procedure... 38

Figure 4.1: Schematic of a basic SEM Colum 40
Figure 4.2: Cross sectional schematic of the primary excitation volume [26]..................................... 43
Figure 4.3: Schematic of a basic TEM Colum 49
Figure 4.4: Scattering of an incident beam of electrons [25] 51
Figure 4.5: Schematic representation of diffraction in TEM.. 53
Figure 4.6: Schematics of the membrane module situated in the oven (left) and permeation test station (right) 59

Figure 5.1: SE images of seeded supports (a) M1, and (b) M3 62
Figure 5.2: SE images for samples of type M3 seeded (a) once (b) twice (c) thrice and (d) sample of type M1 seeded twice.. 63
Figure 5.3: Plot showing the increase in surface coverage for by Pd seeds with increasing number of seeding steps for M3.. 64
Figure 5.4: SE images of seeded samples (a) M2, and (b) M4 65
Figure 5.5: Plot showing the particle size distribution of seeds on M2 and M4 66
Figure 5.6: SE images of (a) blank support and (b) sample M5 68
Figure 5.7: Bright field TEM images of (a) seeds on the support, (b) the seed distribution and (c) SAD pattern of seeds for samples M1 and M3.. 70
Figure 5.8: A typical EDS spectrum for samples M1 and M3 71
Figure 5.9: Bright field TEM images of (a) seeds on the support, (b) typical Pd clusters and (c) SAD pattern of clusters for samples M2 and M4 72
Figure 5.10: A typical EDS spectrum for samples M2 and M4 73
Figure 5.11: SE images of plated samples (a) M1, (b) M2, (c) M3, (d) M4 and (e) M5 76
Figure 5.12: Permeance results for samples A0-A3 using nitrogen gas at room temperature 82
Figure 5.13: Permeance results for samples A2 and A3 at 320°C 83

UNIVERSITY of the
WESTERN CAPE

List of tables:

Table 1.1: Summary of the technologies used for H_2 production [2] 2

Table 2.1: Linear thermal expansion coefficients for various materials at room temperature [1] 10
Table 2.2: Summary of properties for supports used in Pd membrane fabrication 13
Table 2.3: Major characteristics of various techniques used to fabricate Pd membranes. 17
Table 2.4: Effects of osmosis on microstructure of plated films [10] 21

Table 3.1: List of chemicals and materials used during sample preparation 30
Table 3.2: Support information 31
Table 3.3: Composition of the solutions used in the seeding methods 1 and 2. 33
Table 3.4: Composition of the sensitisation, activation and acceleration bath solutions used in the seeding method 3 35
Table 3.5: Composition of the plating bath solution 37

Table 5.1: List of all the seeded supports fabricated in this study 61
Table 5.2: Coverage obtained during seeding 64
Table 5.3: Plot showing the increase in surface coverage for by Pd seeds with increasing number of seeding steps for M3 64
Table 5.4: Support coverage of samples M2 and M4 67
Table 5.5: Elemental composition of various areas of sample M5 69
Table 5.6: Particle size ranges for samples M1 and M3 71
Table 5.7: Void size ranges for samples M1-M5 77
Table 5.8: Characteristics of the plated film microstructure. 77
Table 5.9: Characteristics of the ELP membranes subjected to permeance testing 81
Table 5.10: Selectivity of samples A2 and A3 83
Table 5.11: Permeance results for ZrO_2 supported membranes Z0 to Z4 83

UNIVERSITY of the
WESTERN CAPE

Chapter 1: Introduction

This introductory chapter discusses the production methods and suitability of palladium membranes in the ever growing H_2 economy. Section 1.1 highlights the current industrial based methods for the production of Hydrogen (H_2). Section 1.2 focusses on gas separation technologies and section 1.3 describes the current problems associated with Pd based membranes applied in H_2 production processes and possible remedies.

1.1 Hydrogen Production

H_2 is currently extensively used in the chemical industry, but it is also recognized as the fuel of the future [1, 2, 3]. H_2 can be produced in various ways namely, water electrolysis, photolysis, steam reforming (SR) and gasification of hydrocarbons [1]. Most of the industrial H_2 is produced via SR [1, 2, 3, 4]. SR processes is done via partial oxidation (POX) and auto thermal reforming (ATR) [2]. As shown in Fig. 1.1 methane SR is annually responsible for approximately 50% of the H_2 produced globally. Table 1.1, shows the thermal efficiencies based on the higher heating values of the current technologies employed for H_2 production.

UNIVERSITY of the
WESTERN CAPE

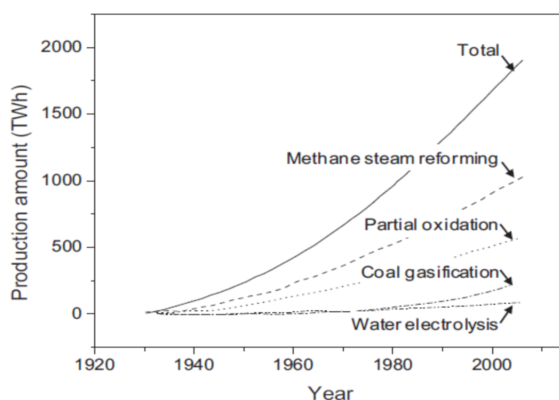

Figure 1.1: Annual global H_2 production using various industrial techniques [1]

Table 1.1: Summary of the technologies used for H_2 production [2]

Technology	Feed Stock	Thermal Efficiency	Status
SR	Hydrocarbons	70-85%	Current
POX	Hydrocarbons	60-75%	Current
ATR	Hydrocarbons	60-75%	near-term
Photolysis	Sunlight + water	0.50%	long-term

Table 1.1 shows that methane steam reforming is also the most effeicient process both currently as well as when compared to possible future H_2 production technologies such as ATR and photolysis. Due to the high efficiency of SR it is easy to understand why this process accounts for the vast majority of H_2 produced annually.

UNIVERSITY of the WESTERN CAPE

Steam reforming reactors employ a two-step process which proceeds as follows. The first step given in equation 1.1 details the formation of syngas (CO and H_2) through an endothermic reaction between methane gas and steam [2]. This reaction requires temperatures above 500°C for efficient hydrocarbon conversion [2]. The second step shown in equation 1.2 is known as the water gas shift (WGS) reaction, in which carbon monoxide (CO) reacts with steam to further produce H_2 as well as carbon dioxide (CO_2). As the water gas shift reaction is exothermic, its thermo dynamic equilibrium shifts towards product formation with decreasing temperature. Typically high temperatures are desired to achieve fast kinetics, but results in high CO formation and decreased H_2 production due to a shift in the equilibrium. In practice this means that two water gas shift reactors are needed; a high temperature WGS (HTWGS) to convert the majority of the CO to CO_2 and H_2O and a low temperature WGS (LTWGS) reactor to convert the CO present in the product stream of the

HTWGS reactor as a result of the thermodynamic equilibrium [2]. The final quantity of CO is then removed further downstream using processes such as pressure swing absorption (PSA) or preferential oxidation (PROX).

The overall reaction is given by equation 1.3. The product gas is a mixture of H_2, CO, CO_2, H_2O and CH_4 [2]:

$$CH_4 + H_2O \leftrightarrow CO + 3H_2 \quad (1.1)$$

$$CO + H_2O \leftrightarrow CO_2 + H_2 \quad (1.2)$$

$$CH_4 + 2H_2O \leftrightarrow CO_2 + 4H_2 \quad (1.3)$$

1.2 Gas Separation Technology

In order to extract H_2 from the reaction mixture, various types of gas separation technologies are used; the most common methods are solvent absorption, PSA, cryogenic recovery and membrane separation [1]. The membrane separation process comes with a greater number of advantages compared to other above mentioned techniques, as it is the most cost effective as well as lowers energy consumption [1]. For these reasons it is viewed as a promising method for meeting the increasing demand of high purity H_2 [1].

UNIVERSITY of the
WESTERN CAPE

Amongst different membrane types, Pd membranes show exceptionally high selectivity towards H_2 and can be used to facilitate the removal of H_2 in the CH_4 SR reactors. Even though other metals such as nickel, platinum as well as some other metals in groups III-V of the periodic table can be used to dissociate and dissolve H_2, Pd displays superior H_2 solubility and selectivity characteristics [1]. The superior solubility and selectivity characteristics of Pd based membranes allow H_2 gas to transport through the metal bulk at a

faster rate, over a wider temperature range than the previously mentioned metals as shown in Fig. 1.2 [1, 4].

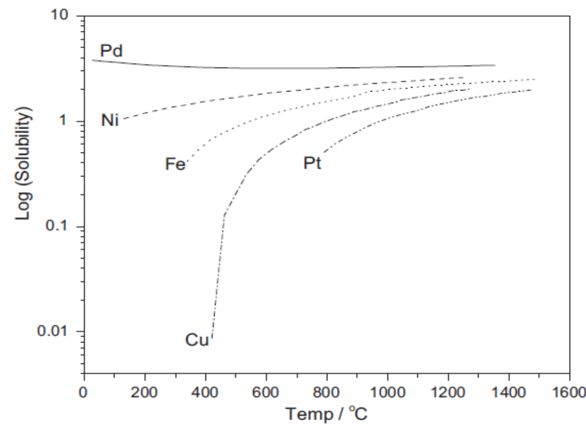

Figure 1.2: Comparison of H_2 solubility for various metals at a pressure of 1 atm [1].

Pd membranes are typically operated between 300 - 600°C, very close to the operating temperatures of the SR and WGS systems. When a Pd membrane is configured as a SR or WGS reactor, a so called "membrane reactor", high purity H_2 is produced at the permeate side of the membrane. Conversions of both CH_4 and CO towards the production of H_2 are no longer limited by their thermodynamic equilibrium as the removal of H_2 from the products in equation 3 shifts the reaction equilibrium in the direction of H_2 formation [4]. As a consequence, the WGS reaction could be performed at high temperatures, with potentially great conversion and production rates without the need for additional H_2 purification technology further downstream in the reactor.

Despite the great potential that Pd membranes offer in H_2 production processes, there are a number of challenges to be overcome before Pd membranes or Pd membrane reactors are implemented throughout the hydrogen production and purification industry. The next section will highlight the current constraints.

UNIVERSITY of the
WESTERN CAPE

1.3 Current problems associated with Pd based membrane

Even though Pd is recognised for its potential use in membrane separation technologies, the metal does suffer from several limitations. When H_2 is absorbed by the metal below the critical temperature of 298^{0}C, an increase in the lattice parameter of the face-centred cubic (FCC) structure is observed [1]. Two different phases, α and β, can be formed. Both phases retain the FCC structure of pure Pd but an increases in the lattice parameter from 0.3890nm to 0.3895nm is observed for the α phase [1]. An even larger increase to 0.410nm is observed for the β phase which occurs at room temperature [1]. These increases in the lattice parameter cause changes in the volume of the metal and gives rise to strain which leads to the formation of grain boundary defects [1]. Continuous exposure of the metal to H_2 leads to a process known as H_2 embrittlement, which causes the metal to crack. The metal thus loses its ductility, due to the constant absorption and desorption cycles of atomic H through the metal [1].

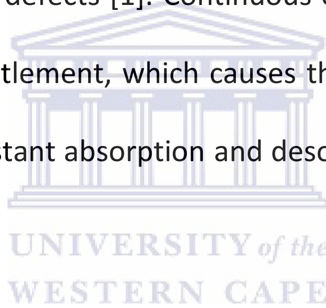
UNIVERSITY of the
WESTERN CAPE

Current H_2 production is derived primarily from the use of natural gas. Other feedstocks used for H_2 production include propane, methanol and coal to name a few. All these chemicals mentioned are carbon derivatives and, with the exception of methanol they also contain small amounts of sulphur (S) [2]. The metallic nature of Pd gives rise to interactions with the carbon containing species and sulphur that deactivates the films surface and affects membrane performance [1]. This is known as film poisoning. In the case of S, the formation of a Pd-S layer that is impermeable to H_2 is often formed on top of the Pd layer [1, 2]. Although Pd-S layers can be removed to restore the performance of the membrane, such procedures do incur unlikely costs.

In order to avoid poisoning and H_2 embrittlement, Pd is often alloyed with various other metals. Alloying with silver (Ag) lowers the critical temperature at which phase transitions occur [1]. Pd alloys formed with copper (Cu) are the most promising in terms of membrane permeance [1]. When alloyed with gold (Au) the Pd-Au membranes show high resistance towards S poisoning [1]. Since each alloy shows an improvement in different aspects of the membrane the next challenge is in finding tertiary alloys to further improve membrane properties [1]. However the use of alloys has its own challenges. Additional metals add to fabrication costs, especially when expensive metals such as gold need to be employed. The additions of more metals also lead to complicated multistep fabrication procedures which increase fabrication costs. There is also the possibility of intermetallic diffusion that destroys the integrity of the membrane [1]. Finally we also have the support fabrication which is a costly operation when trying to fabricate an optimal support with the desired properties for high quality membrane fabrication.

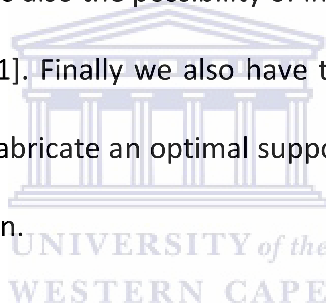
UNIVERSITY of the
WESTERN CAPE

The realisation of commercial Pd membrane application requires

1. Reasonable membrane costs for both the support and the Pd film
2. High H_2 permeance
3. High H_2 selectivity
4. Resistance to poisoning effects
5. Steady and predictable performance over long time periods

Thus the goal is to prepare thin defect free Pd membranes, with high permeability and H_2 selectivity that is chemically stable and thermally durable over long periods [1].

Chapter two will review the available Pd film synthesis techniques, and will show the necessity of a proper seeding method that is applied prior to electroless plating procedure. An understanding of seed formation is deemed necessary as the seeds are seen as the foundation of the Pd film and therefore have a great impact on the performance of the Pd film.

UNIVERSITY of the
WESTERN CAPE

Chapter 2: Literature Review

Throughout this chapter, backgrounds on the membrane supports, seeding methods, surface functionalization, H_2 permeation studies as well as the aims of this study will be discussed. Section 2.1 is related to the choice of an appropriate support in Pd membrane processing. Section 2.2 discusses various methods used in Pd membranes fabrication. Section 2.3 – 2.6 covers the fundamentals and methods of seeding, surface functionalization, as well as H_2 permeation in Pd membranes respectively. Section 2.7 concludes the chapter by outlining the aims of this study based on the findings in the literature.

2.1 Support Selection

2.1.1 Introduction

UNIVERSITY of the
WESTERN CAPE

Pd based membranes can be split into two categories namely self-supported, i.e. unsupported, and supported membranes. Unsupported membranes produce ultra-high purity H_2 and may be more suited for the laboratory where the intrinsic properties of the material can be studied [1]. The main disadvantage with unsupported membranes is that they have to be relatively thick, hundreds of microns, to achieve the required mechanical stability [1, 5]. Since the flow of hydrogen through a specific unit of surface area is indirectly proportional to the film thickness [1, 6, 7], thicker films require a larger surface area to achieve the targeted permeation rates.

Due to the considerably high cost of Pd, unsupported membranes are not suitable for industrial applications. The thick Pd layer required by unsupported membranes also lowers

the permeability [1, 5]. Unsupported membranes are initially obtained through the use of a support which is mechanically removed once the film of Pd has been deposited [1].

Supported membranes are fabricated by depositing a thin dense film of uniform thickness around 1-20μm on a porous support. These types of membranes are the focus of recent research, as higher H_2 fluxes can be achieved with thinner Pd layers, and the cost of material fabrication is lowered when compared to unsupported Pd membranes [1, 5]. A dense film is one that exhibits no defects, like pin holes and voids, and displays infinite selectivity towards H_2. The selectivity of a Pd membrane is defined as the ratio of H_2 to N_2 permeance through the membrane. When a membrane displays zero N_2 permeance, it is said to be infinitely selective. The requirement of meeting both the necessary H_2 selectivity and permeability may be obtained through the use of supported membranes, while the reduced amount of Pd material required to fabricate the membrane may be off set against the support cost.

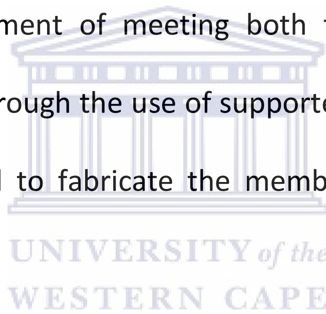
UNIVERSITY of the
WESTERN CAPE

Porous supports used for Pd membrane fabrication, can generally be divided into two main types. These include porous metal and porous ceramic supports. Both types of supports have been used successfully for the deposition of dense Pd and Pd-alloy films [1]. The discussion that follows focuses on the advantages and disadvantages for each type of support with the focus mainly on their suitability for use in methane steam reforming reactions.

2.1.2 Types of Pd membrane supports

2.1.2.1 Porous metal supports

The porous metal supports (PMS) are electrically conductive, with a typical pore size range of 0.5-100 μm in commercially available supports [5, 8]. These supports can be fabricated

into various geometries such as flat disks or tubes [1, 5]. The most commonly used PMS is the porous stainless steel (PSS) support [1, 5]. An advantage of these supports is that sturdy and gas tight seals are achieved with relative ease [1, 5]. This is an attractive feature for industrial membrane assemblies. Another attractive feature of PMS is that they have a linear thermal expansion co-efficient similar to that of Pd as shown in table 2.1.

Table 2.1: Linear thermal expansion coefficients for various materials at room temperature [1]

Material	**Linear thermal expansion coefficient (10^{-6} K^{-1})**
Alumina	5.4-6.7
Borosilicate glass	3.3
Palladium	11.8
Stainless Steel	11-16

UNIVERSITY of the WESTERN CAPE

This is important during any thin film fabrication, as thermal stresses caused during expansion and relaxation of the different lattices, could lead to the degradation of the membrane [1, 5].

The greatest drawback of MPS is that metallic supports are subject to intermetallic diffusion [1, 5]. Intermetallic diffusion is the process whereby metal atoms of the support diffuse into the Pd based layer. The presence of these metal atoms in the Pd layer eventually degrades the properties of the membrane. Since the diffusion rate of the metal atoms is related to the melting point of the metal, the operational temperature range for metal supported Pd films is typically below 600°C. The problem of intermetallic diffusion can however be

suppressed through the creation of diffusion barriers, which to a certain degree prohibit the migration of metal ions from the support into the Pd film [8].

Although MPS supports offer good mechanical durability, good adhesion, and good seal properties, the operational temperature below 600°C limits their suitability for industrial processes such as methane SR. A number of publications have confirmed the limited durability of PSS supported Pd membranes specifically at 600°C; a minimum temperature of 600°C is required in CH_4 steam reforming. Despite the introduction of the intermetallic diffusion barriers, the durability remains a serious concern [1, 5, 6]

2.1.2.2 Ceramic Supports

2.1.2.2.1 Porous Glass Supports

Porous Vycor glass is the most common amongst porous glass supports (PGS), and was one of the first materials used as a support for the fabrication of Pd membranes [1]. Whilst these supports are able to operate at relatively high temperatures, between 300°C and 450°C, their greatest drawback is that they form Pd membranes that are mechanically fragile. The smooth surfaces exhibited by these supports do not provide adequate adhesion to the Pd film deposited onto them [1, 5, 9]. Poor adhesion can however be overcome by incorporating techniques such as osmosis into the fabrication process. When osmotic pressure is applied during seeding the Pd nuclei penetrate deeper into the porous support. This causes the formation of intermediate zones of gradually changing Pd-SiO_2 compositions during plating [9].

The use of osmosis, and similar variations, is also unfavourable as they add significantly to the cost of membrane fabrication. The limited thermal stability, mechanical fragility and

UNIVERSITY of the WESTERN CAPE

poor adhesion to the top layer Pd film makes PGS unattractive for use in Pd membrane fabrication.

2.1.2.2.1 Porous Alumina (Al_2O_3) and Zirconia (ZrO_2) supports

Porous Alumina (Al_2O_3) and Zirconia (ZrO_2) supports are non-metallic, and can be formed into various shapes, but with the added advantage of controllable pore sizes [1, 5]. These supports also offer good mechanical and thermal stability, and thus are suitable for application in existing industrial applications such as SR and pressure swing absorption [10].

These supports are often used in the fabrication of composite membranes. Due to large pore sizes exhibited by commercial PSS supports, either ZrO_2 or Al_2O_3 layers are deposited onto the PSS to reduce pore sizes as well as the mean-flow pore sizes of the membrane [8]. After the deposition of the Pd film on top of ZrO_2 or Al_2O_3 layers, they also serve as diffusions barriers between the two metals [8]. Typical pore diameters for both these type of supports are around less than 150nm [11]. Both ZrO_2 and Al_2O_3 are inert surfaces. This characteristic makes them favourable for use in chemical vapour deposition (CVD) techniques as they are able to achieve higher Pd loading when compared to other supports [8].

UNIVERSITY of the WESTERN CAPE

A drawback of the alumina supports is that during long term permeance testing at temperatures above 600°C, a decrease in H_2 permeance is often observed [12, 13]. This decrease in the permeance is attributed to a Pd-Al alloy formation [12, 13]. The highly active atomic H found at the support-film interface is said to reduce the Al_2O_3 to Al, thus allowing the Al to migrate into the Pd layer and form the alloy that is impermeable to H_2 [12, 13]. It was concluded that atomic H was the reason for the Pd-Al alloy formation as alloy formation was not observed when argon gas was used under similar conditions [13]. However no such

interaction was observed when yttiria–stabilised zirconia (YSZ) supports were used. The YSZ supported Pd membranes exhibited steady permeation when tested at 650°C for 334h [13]. This demonstrates the enhanced suitability of YSZ supports for use in SR reactors, when compared to alumina supports.

The greatest drawback of these type of ceramic supports is the difficulty to obtain gas tight seals with them [1, 5], even though glass or graphite seals are quite common.

2.1.3 Characteristics of various supports

A list of characteristics for the various supports discussed in sections 2.1.2-4 is given in table 2.2.

Table 1.2: Summary of properties for supports used in Pd membrane fabrication

Support Type	Name	Advantages	Disadvantages
Metal	SS	Easy to seal	Limited thermal stability at 600°C
		Mechanical stability	
Ceramic	Glass		Limited thermal stability at 600°C
			Mechanically fragile
			Poor Pd deposit adhesion
	Al_2O_3	Mechanical stability	Limited thermal stability at 600°C
			Not easy to seal
	ZrO_2	Mechanical and thermal stability	Not easy to seal

UNIVERSITY of the WESTERN CAPE

Due to the robust characteristics of the ZrO_2 supports, the fabrication of Pd membranes using these supports are thus a promising prospect.

2.2 Introduction to Pd Membrane Fabrication

There are various techniques for processing palladium (Pd) membranes. These include Chemical Vapour Deposition (CVD), Physical Vapour Deposition (PVD), Electroplating (EPD) as well as Electroless Plating (ELP) [1, 5]. These techniques are discussed in the following sections in relation to membrane processing.

2.2.1 Chemical Vapour Deposition technique

This process involves the thermal decomposition of a metal complex, usually in the gas phase. Thermal decomposition of the metal precursor allows metal ions to deposit onto the surface of the substrate and grow as a thin film. The precursor material needs to be highly volatile and for this reason the precursor is usually an organometallic. The metal complex is usually sublimed in a separate chamber and is transported by means of a carrier gas to the substrate. The gas is then thermally decomposed and the resulting ions and/or radicals deposits as a thin film on the support surface through nucleation. [1, 5, 6].

UNIVERSITY of the
WESTERN CAPE

The CVD method offers various advantages over other techniques. One of the advantages is that this process is attractive for obtaining Pd layers of controlled thickness during the deposition of both pure Pd and Pd-alloy layers. Jun et al [14] have used the metallo-organic chemical vapour deposition (MOCVD) to successfully deposit reproducible Pd and Pd-Ni alloy composite membranes with thickness ranging from 0.5 µm to 1 µm. Although the membranes obtained did not exhibit good H_2/N_2 selectivity and low H_2 fluxes, their work portrays the high level of control that can be obtained in the Pd films thickness and composition when using the CVD technique.

Itoh et al. [15] used the CVD technique in combination with precursor forced flow. This allowed for simultaneous precursor decomposition and Pd deposition in the pores of the

substrate due to the pressure difference applied between the outside and inside of the support. This resulted in thin film Pd membranes of thickness between 2-4 µm that exhibited high H_2 flux as well as a H_2/N_2 selectivity of 5000.

The greatest drawback of this technique is the high fabrication cost. The CVD process requires complex equipment such as vacuum pumps and special heaters, to meet the strict process conditions required for thin film fabrication. The scale-up of the systems for industrial production remains a challenging task; for this reason the CVD process is best suited to laboratory work for the optimization of the deposition parameters [1, 5]. The volatile and thermally stable precursors required for CVD are expensive. Contamination of the sample is also possible if the strict process conditions of this technique are not adhered to [1].

2.2.2 Physical Vapour Deposition technique

UNIVERSITY of the
WESTERN CAPE

In physical vapour deposition (PVD) it is found that the precursor material, usually a solid, is evaporated, or decomposed, by physical means such as sputtering under high vacuum [1, 5]. An example of PVD processes is the magnetron sputtering technique. Ryi et al. [16] have used magnetron sputtering to produce dense ternary Pd-Cu-Ni films around 4 µm thick. It is also reported that the membranes fabricated in their study exhibited high selectivity, as the nitrogen flow rate through the membranes was negligible. The fabricated membranes showed good stability, with no evidence of metallic inter-diffusion, between the three metal layers, when operated in the $300^{o}C$ - $500^{o}C$ at temperature range.

Although the PVD technique presents many advantages, a disadvantage is its suitability only for flat supports. Similarly to CVD, this technique is also best suited for the laboratory as it also requires specialised equipment and strict process conditions.

2.2.3 Electroplating technique

Electroplating deposition (EPD) is an electrochemical process in which the support is used as a cathode. The positive metal ions are transported by means of an electrical potential, and deposited onto the support. The thickness of the film can be controlled by tuning the deposition times and current density [1, 5]. Chen et al. [17] have reported the successful fabrication of a defect free Pd membrane with a H_2/N_2 selectivity greater than one million.

Porous Stainless Steel (PSS) is commonly used as a support for this technique, because the support used in EPD also serves as an electrode [1, 18]. This is a disadvantage of the EPD technique as the support and all its components, such as diffusion barriers, are required to be conductive [1, 5, 6]. The advantages for EPD include easy set-up and process procedure; there is neither any restriction on the geometry of the support to be used. [1, 5].

2.2.4 Electroless Plating technique

UNIVERSITY of the
WESTERN CAPE

The electroless plating (ELP) fabrication method involves the reduction of metal complex ions on the target/support surface by the aid of a reducing agent. The process is carried out in two steps (a) Seeding, also known as activation, and (b) plating. Metal sites formed during the seeding process acts as a catalyst, and provide the initial platforms for the metal plating. ELP is the preferred choice for Pd membrane fabrication, due to its ease of coating on supports of various geometries [1, 5, 6]. This technique is effective and low in cost as it requires a simple setup [1, 5].

One of the drawbacks of ELP is that it is a time consuming technique [1, 5]. During the seeding process, a multistep procedure has to be repeated several times in order to ensure that proper activation is achieved, which promotes film growth during the plating procedure. Another drawback is that although the technique yields uniform film deposition,

it does not offer adequate control over the thickness of the film being deposited [1, 5, 6]. A summary of the characteristics for the formerly mentioned Pd membrane fabrication techniques is given in table 2.3.

Table 2.3: Major characteristics of various techniques used to fabricate Pd membranes.

Fabrication Technique	Advantages	Disadvantages
CVD	produces high quality membranes	high in cost suitable for the laboratory
PVD	produces high quality membranes	Limited support geometry high in cost suitable for the laboratory only
EPD	simple setup uses any shape of support cost effective	supports have to be conductive
ELP	simple setup uses any type and shape of support cost effective	time consuming fabrication procedures Difficult to control film thickness

UNIVERSITY of the
WESTERN CAPE

Provided that fabrication steps can be simplified, ELP has valuable advantages over all other methods. Due to the promise that ELP holds in Pd membranes processing, it has been used to produce the samples investigated in this study.

2.3 Seeding

2.3.1 Introduction

As it transpires from the above discussion, the ELP technique can be used to plate metallic films on various types of supports [1, 5, 6]. It is a bottom-up approach by which the thin film is formed by metal atom deposition [18, 19]. This electrochemical process is governed by a heterogeneous reaction as the electron transfer during metal deposition occurs at the solid-liquid interface between the surface of the support and the solution [6, 7]. The process is

autocatalytic, in which the "voltage/current" is supplied by the chemical reduction of the metal near the support surface [18, 19].

A standard industrial practice for the ELP process involves the seeding of the support [7, 9]. Seeding also referred to as surface activation or nucleation, which is the initial deposition of small islands of metal nuclei on the support surface. The quality of a Pd film on top of an activated substrate, in terms of film adhesion, coverage and density, is dependent on the roughness of the support as well as the coverage of the support by the Pd seed particles. [20].

2.3.2 Impact of seeding on plating

As seeding is the first step in the ELP process, it greatly influences the metal film deposited on the surface of the support. Seeding influences the efficiency of the plating procedure, the thin film microstructure and film adhesion.

UNIVERSITY of the
WESTERN CAPE

Sun et. al. [21] reported that the surface properties of the support greatly affect the surface morphologies of Pd membranes. They presented results obtained from three different supports of varying surface roughness. The support that exhibited the largest amount of roughness, produced a Pd film with the least uniformity, likewise the support with the smallest roughness profile exhibited increased uniformity in the Pd film formed. Due to the varying locations of the seeds on the support, the probability of metal deposition at various sites will differ significantly. For seeds located at the hills of the roughness profile, the probability of plating will be higher than for those seeds located in the valleys or elsewhere. Thus it is reasonable to expect that if all the seeds have the same probability of plating, for flat and smooth surfaces, the microstructure of the film that forms will be more uniform [9].

Since the metal nuclei formed in seeding provide the catalytic surfaces for further metal plating, a properly activated surface reduces the induction period, i.e. the time at which plating procedure actually begins, and also initially increases the metal deposition rate [7, 9]. This results in an improved plating efficiency.

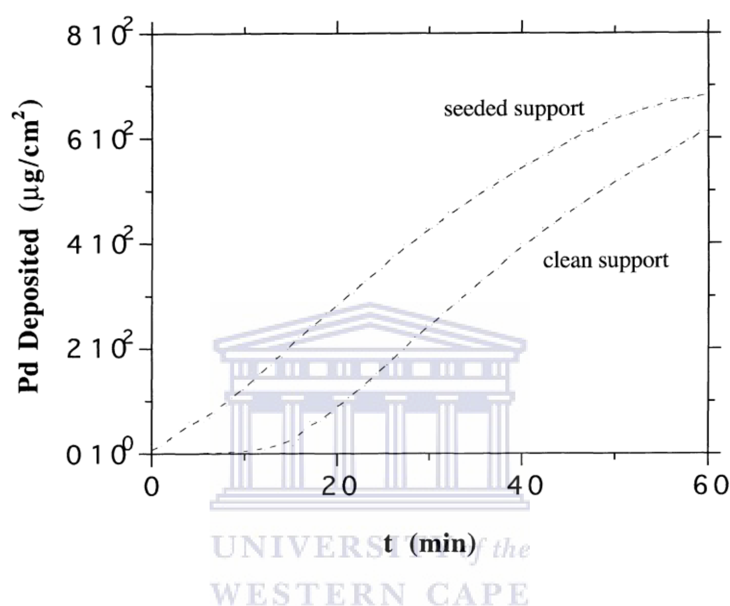

UNIVERSITY of the
WESTERN CAPE

Figure 2.1: Comparison between the deposition rates on seeded and clean supports [7]

Figure 2.1 compares the deposition rates on seeded and clean supports. The curves show that a higher deposition rate is observed on the seeded support although the plots come closer after roughly one hour of deposition when the saturation point has been reached. At this point Pd deposition is slower as either the availability of Pd in the plating bath is slowly depleting or by means of reduced catalytic activity exhibited by the stabilised deposited film. Even at this stage the deposition rate on the seeded support is still higher. The use of ELP on activated supports aims to optimize the density of the processed membrane with a minimal thickness; higher deposition rates are thus not a crucial issue in these studies.

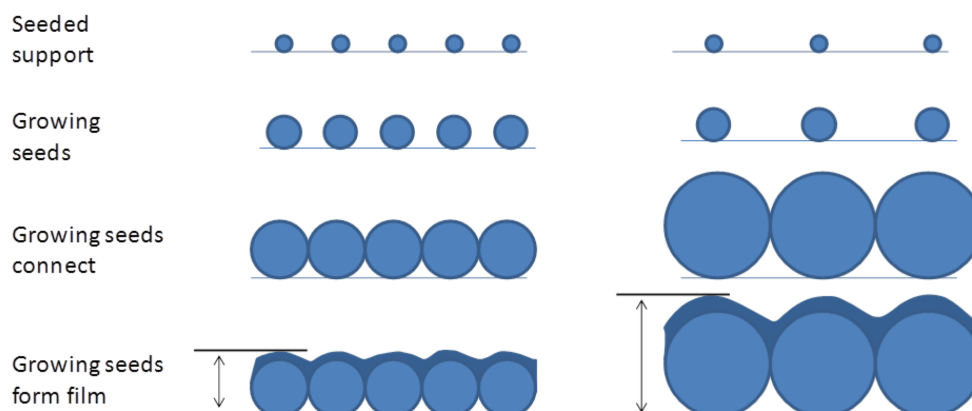

Figure 2.2: Illustration of film formation during plating

Figure 2.2 shows an illustration of film formation during plating. During the initial stages of plating preferential metal deposition occurs at the seeds [6, 9, 21]. Over time the seeds increase in size and start to overlap. After connecting, further metal deposition occurs uniformly over the connected seed areas. From figure 2.2 assuming the support area is flat and smooth, the formation of thin Pd layers are thus dependant on both the number and the distribution of the Pd seeds [20, 21].

UNIVERSITY of the
WESTERN CAPE

The influence that seeding has on the film microstructure is also important. If the seeded support exhibits non-uniformity due to factors like the topography of the support's surface, this will result in the non-uniformity of the microstructure of the film formed [9].

The effect of osmosis on the formation of film microstructure has been studied in the work done by Suleimanova et al. [9]. In this study, osmosis is employed in both the seeding and plating procedures, and the results are compared to those obtained when processing Pd membranes without osmosis.

Table 2.4: Effects of osmosis on microstructure of plated films [10]

Procedure	Average grain size (nm)	Width of size distribution (nm)
Seeding and plating without osmosis	760	25
Seeding with osmosis and plating without osmosis	720	18
Seeding and plating with osmosis	480	13

Table 2.4 shows the results obtained in the study. With the use of osmosis during seeding the distribution of Pd in the support is increased significantly and distributed more uniformly throughout the support. The result is a Pd film of finer grain size, and increased uniformity as seen by the size distribution when compared to a membrane fabricated without osmosis. The result is even more uniform film when osmosis was used in both the seeding and plating procedures.

UNIVERSITY of the
WESTERN CAPE

Seeding also plays an important role in improving the adhesion between the support and the plated film [9]. By allowing the Pd seeds to penetrate deeper, the film is allowed to further integrate into the support. Integration is easily obtained when using osmosis, and further strengthens the adhesion between the film and support. This phenomenon was qualitatively shown by Suleimanova et al [9].

Seeding is thus an important component of the ELP process. In many ways, it directly influences the initial plating process, which in-turn determines the characteristics of the final membrane.

2.4 Seeding Methods

The most commonly used method known as the sensitization-activation cycle [6, 9, 22, 23], is discussed in section 2.4.1. The drawbacks of the sensitization-activation cycle method are found in section 2.4.2. Other modified seeding methods are discussed in section 2.4.3.

2.4.1 $SnCl_2$-$PdCl_2$ based Methods

This procedure makes use of a colloidal $SnCl_2$ solution as the sensitizer, and a Pd precursor solution, usually $PdCl_2$, as the active species. This process typically involves the sequential submerging of the support first in the sensitisation solution, then rinsing in water, followed by submerging the support in acidic activation solution, and finishing the cycle by rinsing with deionized water. This cycle is often repeated numerous times, between five to ten times, to ensure sufficient uniform coverage of the support surface with catalytic Pd nucleation sites. A modified version of this method consists in placing both the sensitizer and activator in the same bath. This helps to reduce the time consuming nature of the activation cycle [6].

UNIVERSITY of the
WESTERN CAPE

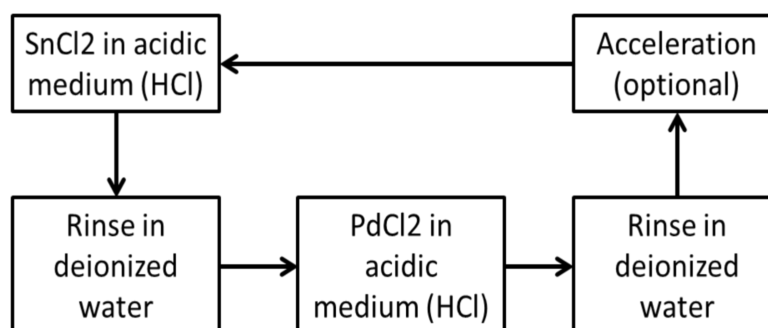

Figure 2.3: Schematic of the steps followed during the sensitisation- activation cycle

In the sensitisation-activation cycle, the Sn is employed to anchor the Pd to the surface of the support. During the immersion of the support into the acidic Pd solution, the Sn binds to

the Pd forming a Sn-Pd alloy at the surface of the support. This binding mechanism is illustrated in Fig. 2.4.

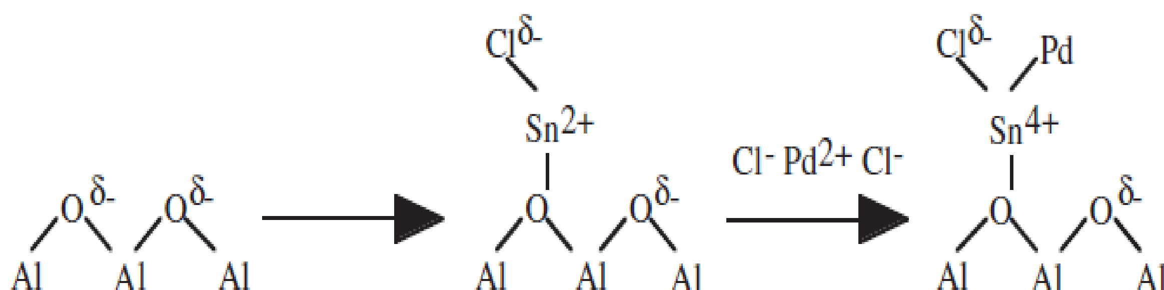

Figure 2.4: Schematic representation for Pd attachment to alumina support [16]

The binding of the Pd to the support surface is mediated by Sn^{4+} through the following equation [6]:

$$Sn^{2+} + Pd^{2+} \rightarrow Sn^{4+} + Pd^{0}. \quad (2.1)$$

UNIVERSITY of the
WESTERN CAPE

Equation 2.1 suggests that all Sn^{4+} ions formed after the Pd atoms have been anchored to the support, should be dissolved by the acidic medium of the Pd activation solution. However Sn rich surfaces usually cover the active Pd sites with levels varying according to the Pd/Sn ratio in the various baths [6]. The formation of Sn rich surfaces on top of the Pd seed sites thus hinders the catalytic activity of the seeds during plating [6, 23].

A further improvement to this procedure involves addition of an acceleration step. The acceleration step makes use of an acidic medium, which is employed to help with the removal of excess Sn formed at the Pd-membrane interface and is added to the end of each cycle [6, 24]. Finally the use of rinsing is employed to decrease the transfer of contaminants, excess Sn and Pd, to the plating baths. These contaminants would cause spontaneous decomposition of the plating bath due to the presence of the reducing agent [6].

2.4.2 Drawbacks of the $SnCl_2$-$PdCl_2$ based seeding method

The presence of Sn in the activation of a Pd membrane is not favourable due to its hindrance of the plating procedure. A study by Collins et al. [23] shows the negative influence it has on the resulting Pd membrane, through the investigation of the performance of three types of different membranes. In this study two of the three types of membranes fabricated made use of the conventional Sn/Pd sensitisation-activation procedure in comparison to the third which was activated using a tin less seeding procedure. Two of the membranes prepared by the conventional method differed by the amount of Sn used in the seeding procedure; we refer to them as type 1 and type 2. Type 1 used a full strength Sn bath, whilst type 2 made use of a Sn bath that contains 100 times less Sn than what was found in the bath of type 1. The support activated in a bath containing no Sn will be referred to as type 3.

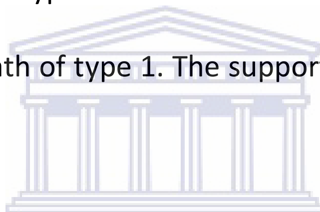
WESTERN CAPE

It was found that the H_2/N_2 selectivity of the membranes seeded with Sn decreased rapidly over time, when tested at temperatures around 500°C. This decrease in selectivity is more prominent in type 1 membranes, obtained from a full strength Sn bath, than in type 2 membranes, the dilute Sn bath. The type 3 membranes, no Sn in the activation bath, were able to maintain their selectivity even when tested at a temperature of 600°C. Selectivity of the type 3 membranes was also well maintained for longer operating periods. The results displayed by type 3 membranes are favourable when considering Pd membranes for use in steam reforming, and show that the presence of Sn on the membrane is detrimental to its quality and long term stability.

2.4.3 Modified Seeding Methods

Modifications to the seeding procedure have been employed in the membrane fabrication process. These can be split into two types which relate to different seeding methodology and chemistry. A limited number of seeding methods applying alternative chemistries were found.

The first method by Tong et. Al. [11] involves the use of a polymer template into which the Pd seeds were embedded before being placed onto the support. This activated template was then removed again after the plating procedure had been completed. The advantage of this method lies in the fact that a uniform distribution of the seeds in the polymer resulted in a uniform distribution of the seeds on the support once the activated template was placed on top of it. The uniform distribution of the seeds resulted in a smooth 5µm thick Pd film of uniform thickness. The removal of the polymer template after plating also resulted in a small gap between the support and the Pd film, which significantly enhances the permeability of the membrane when compared to a conventionally formed composite membrane.

UNIVERSITY of the
WESTERN CAPE

Due to the deeper penetration of the seeds into the support, mechanical stability of the membrane is also enhanced when osmosis is applied during seeding [9].

Other modified seeding procedures include the use of a Pd seeds impregnated in a boehmite (AlOOH) sol by a sol-gel process [20]. Even though this process produced membranes with the desired properties, the fabrication process is very lengthy and time consuming stretching to a minimum of three days for membrane preparation.

In terms of modified seeding chemistry, Collins et al [23] used Pd acetate (PdOAc) as Pd precursor during the seeding procedure. This alleviated the problem of film instability at elevated temperatures by excluding the use of Sn entirely from the seeding procedure.

2.5 Surface Functionalisation

The use of surface ligands to anchor catalyst particles to a support surface, in this case inorganic material, is very well known [10, 24]. Typically functionalised organosilanes are used as appropriate surface ligands, and form monolayer films on the support surface [24]. The Pd selectively binds to the surface bound ligand to anchor itself to the support surface [10, 24].

Amino-propyl-tri-ethoxy-silane (APTES) has been identified as a suitable surface ligand due to its commercial availability and its simple functionalization mechanism shown in Fig. 2.5 [10]. The amine group in APTES provides a lone pair of electrons to which the Pd^{2+} ions bind during the seeding procedure. The metal ions are then subsequently reduced to metal atoms which deposit onto the support surface.

UNIVERSITY of the
WESTERN CAPE

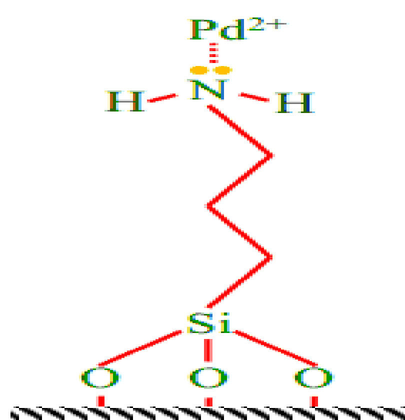

Figure 2.5: Schematic representation for Pd attachment to APTES attached to the support

Due to its selective binding interaction with Pd(II) particles, APTES has the ability to improve adhesion, as well as increase the number and distribution of active Pd sites formed on the support surface during the seeding process [10].

2.6 Permeance study of the palladium coated supports

The quality of a Pd membrane is defined by its perm selectivity towards H_2, the permeance value and its durability [1, 5, 6]. Permeance selectivity tests are used to establish to what extent the membranes contains defects. It also shows the permeance of the membrane

Generally all membranes are subjected to single gas permeation test. These tests are done by using both N_2 and H_2 gas. When a Pd membrane is subjected to H_2 testing, it should be carried out at temperatures above the critical value of 298°C. This is the upper limit temperature at which the Pd film will not undergo an α/β phase transformation, which destroys the integrity of the film [1, 5, 6]. The N_2 permeance is also tested in order to determine the selectivity of the membrane. Ideally the membrane should exhibit zero permeance for N_2. In this instance the membrane is said to be infinitely selective. This is the case for a dense membrane which is defined as being defect free [1, 5, 6]. Due to the mechanism of H_2 diffusion through the metal, discussed in chapter 3, a dense membrane will thus only allow H_2 through and produce a high purity H_2 gas permeate from a mixture of feed gases.

UNIVERSITY of the
WESTERN CAPE

The mechanism of H_2 permeance as well as the theory behind these phenomena will be further discussed in section 3.9.

2.7 Aims and objectives

The aim of this study is to investigate the Pd seeding mechanisms on Al_2O_3 supports. A particular focus will be put on the optimization of

1. the seeds' size distribution and
2. coverage of the support by the seeds.

These properties will be related to different experimental seeding procedures. Plating experiments will be done on differently seeded supports in order to study the resulting microstructure of the films. Focus will also be placed on the use of surface ligands, to investigate their influence on the seeding and plating procedures. The outcomes of their involvement in the processes will thus also be discussed.

2.8 Conclusion and Thesis Outline

2.8.1 Conclusion

The literature review revealed that palladium membranes intended as membrane reactors for steam reforming would be most durable when ZrO_2 supports were used over Al_2O_3 and PSS. If electroless plating were to be selected as a potentially cost effective plating technique, a seeding step will have to be applied. These seeds seem to play an important role in the initiation of the plating and the final quality of the Pd film. The majority of authors refer to the well-known seeding procedure that involved the reduction of Pd with the use of Sn^{2+}. More recent papers have indicated that this Sn^{2+} has a negative effect on the durability of the Pd film, it also appears to reduce the temperature at which a Pd membrane can be operated successfully. Despite the importance of the seeding procedure

and in particular Sn-free seeding methods, a very limited amount of literature is available on the seed formation and seed properties.

2.8.2 Thesis Outline

In chapter 1 a brief summary was given to highlight the suitability of membrane technology for the separation and purification of high purity H_2 using Pd membranes. In this chapter the importance of the appropriate support choice (Al_2O_3 and ZrO_2) and fabrication method (ELP) for Pd membranes were highlighted. The importance of seeding in ELP, as well as the effect it has on the initial plating process, and thus the resulting membranes were also discussed. In chapter 3 the various methods for support activation will be outlined. Chapter 4 will discuss the various analytical techniques used for samples characterization. Chapter 5 presents the results and their discussion. A conclusion as well as suggestions for future work and investigations to be explored will be given in chapter 6 at the end of the thesis.

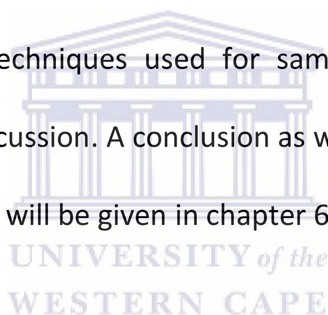

UNIVERSITY of the
WESTERN CAPE

Chapter 3: Experimental Methods

3.1 Materials and chemicals

All materials and chemicals used in this study are listed in Table 3.1. The list also contains the details about the chemicals, as well as the supplier's information.

Table 3.1: List of chemicals and materials used during sample preparation

Materials	Supplier	Details
Alumina (Al_2O_3) Support	Hyflux CEPAration Technologies	High purity aluminium oxide support
Zirconia (ZrO_2) Support	Prepared at SAIAMC	Sintered at 1500^oC
Palladium Chloride ($PdCl_2$)	SA Precious Metals	Palladium precursor
Palladium Acetate (PdOAc)	SA Precious Metals	Palladium precursor
APTES	Industrial Analytical	Used in pre-seeding treatment
Hydrazine Monohydrate (N_2H_4)	Industrial Analytical	Reducing Agent
Chloroform	Industrial Analytical	HPLC grade (solvent)
Hydrochloric Acid (HC)l	KiMix	32%
Nitric Acid (HNO_3)	KiMix	Analytical grade (AR)
Ethanol	KiMix	99% (Absolute)
Sodium Hydoxide (NaOH)	KiMix	Analytical grade (AR)
Ammonium Chloride (NH_4-Cl)	KiMix	Analytical grade (AR)
Ammonium Hydroxide (NH_4-OH)	KiMix	Analytical grade (AR)
Distilled water	UWC	Pure Aqua system

UNIVERSITY of the WESTERN CAPE

Samples were prepared using Al_2O_3 and ZrO_2 supports whose details and characteristics are given in Tables 3.1 and 3.2 respectively; the permeance tests experiments were also carried out on both supports listed in table 3.2.

Table 3.2: Support information

Type (Composition)	Ceramic (Al_2O_3)	Ceramic (ZrO_2)
Inner diameter	1.8mm	0.8mm
Outer diameter	2.8mm	1mm
max Length	200mm	100mm
Average pore size	200nm	-
Type	Symmetric	Asymmetric

UNIVERSITY of the
WESTERN CAPE

3.2 The cleaning procedure of the supports

The cleaning of the support is the first step in the preparation process of Pd membrane fabrication. Cleaning is necessary to ensure the removal of contaminants from the support surface, and to ensure good adhesion and uniform metal deposition.

The HYFLUX supports were cleaved into 0.02m (2cm) long pieces. The separated pieces of support were then sequentially submerged in various solutions for cleaning in an ultra-sonic bath (USB) for 30mins each time. Supports were cleaned ultrasonically in a 0.5 M sodium hydroxide (NaOH) solution, followed by a bath in 0.5 M hydrochloric acid (HCl) solution and thereafter in absolute (99%) ethanol solution. The supports were then rinsed in the USB using distilled water before drying at 130°C overnight. After drying the supports were placed in a desiccator to avoid the adsorption of moisture before activation.

3.3 Seeding

As seeding is the highlight of this investigation, the seeding procedures are described in Sections 3.3.1-3. The Sn free seeding procedures that make use of palladium (II) acetate as the metal precursor, are described in sections 3.3.1-2. The conventional activation-sensitisation method used is outlined in section 3.3.3. Some fabricated samples were also subjected to a pre-seeding treatment which is described in Section 3.3.4.

3.3.1 Seeding Method 1

The first seeding method involves the use of dilute hydrazine N_2H_4 as a reducing agent. The compositions of the seeding solutions used in method 1 and 2 are given in table 3.3.

In the seeding procedure denoted Method 1, the support is submerged in the seed solution, outlined in table 3.3, and hand stirred for 30 seconds. The support is directly dried for 15 minutes at 57°C and at the end it appears to have a reddish tinge. The activated support is then submerged in a dilute N_2H_4 reduction bath outlined in table 3.3 and hand stirred until the evolution of N_2 gas from the support surface has stopped. The activated support is finally dried at 95°C for 15 minutes. The cycle is thereafter repeated numerous times (5-10 cycles) until the support exhibit a uniform black coating. The uniform coating is characteristic of a well activated support. Fig 3.1 shows an outline of the procedure followed in seeding method 1.

UNIVERSITY of the
WESTERN CAPE

Table 3.3: Composition of the solutions used in the seeding methods 1 and 2.

Seeding bath solution:	
$Pd(Ac)_2$	4g/L
Solvent	Chloroform ($CHCl_3$)
Temperature	40˚C
Duration	0.5 mins
Method 1	
N_2H_4	10ml/L
Duration	N2 evolution stops
Method 2	
H_2 gas	bubbling
Duration	15 mins

UNIVERSITY of the
WESTERN CAPE

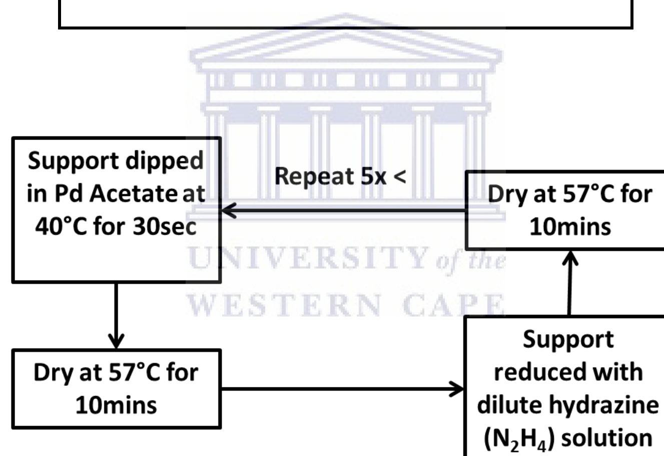

Figure 3.3: Schematic of the procedure for seeding method 1

3.3.2 Seeding Method 2

The second seeding method is similar to the previous one, but it uses H_2 gas as reducing agent. The reduction of the seeded support is then carried out by submerging it in distilled water with continuous stream of H_2 gas bubbling through the solution for 15 minutes. The complete seeding cycle is repeated numerous times (5-10 cycles) until the supports exhibit a

uniform black coating. Fig 3.2 shows an outline of the procedure followed in seeding method 2.

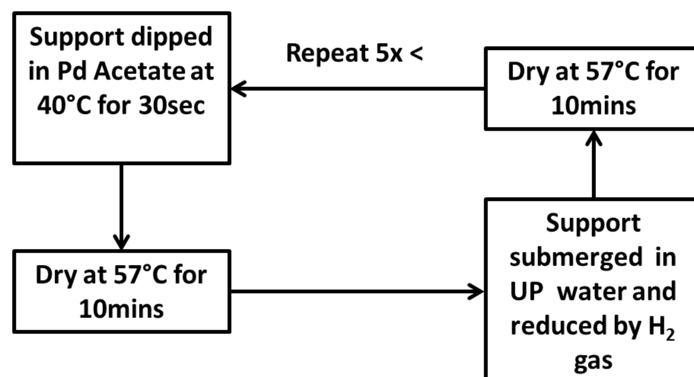

Figure 3.2: Schematic of the procedure for seeding method 2

UNIVERSITY of the
WESTERN CAPE

3.3.3 Seeding Method 3

The third seeding method used was the sensitisation activation cycle. In this method, the support was submerged in a Sn bath with composition as outlined in table 3.4. The support was then removed from the Sn bath after 5 minutes and rinsed in distilled water to remove excess Sn. The support is then placed in a Pd bath outlined in table 3.4 for 5 minutes. The support is then transferred to a 0.01M HCl solution acceleration bath for 1minute. Finally the support rinsed in distilled water for 1minute, and the cycle was repeated 5-10 times until the support exhibits a uniform red-brown coating. Fig 3.3 shows an outline of the procedure followed for seeding method 3.

Table 2.4: Composition of the sensitisation, activation and acceleration bath solutions used in the seeding method 3

Sensitisation bath:	
$SnCl_2$	1g/L
HCl (37%)	1ml/L
Temperature	room temperature
Duration	5 mins
Seeding bath:	
$PdCl_2$	0.1g/L
HCl (37%)	1ml/L
Temperature	room temperature
Duration	5 mins
Acceleration bath:	
HCl (37%)	1ml/L
Duration	1 mins

UNIVERSITY of the
WESTERN CAPE

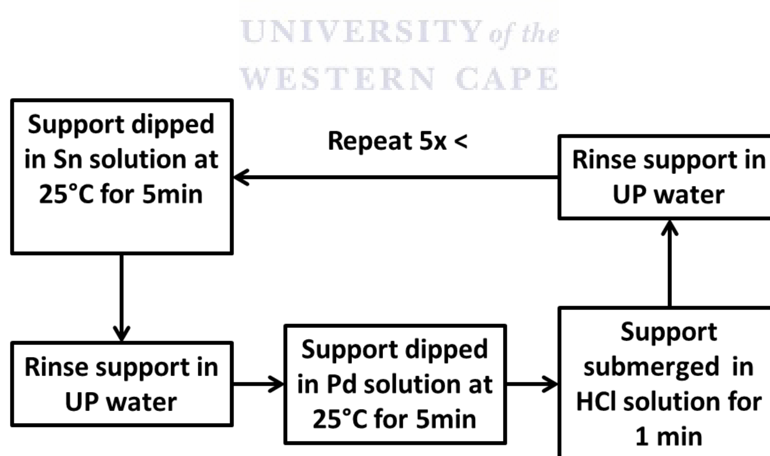

Figure 3.3: Schematic of the procedure for seeding method 3

3.3.4 Pre-seeding treatment

Ligand activation is a process that happens prior to seeding, to ensure the attachment of the surface ligand to the top of the support. This allows for the chemisorption of the Pd seeds

onto the support surface [19]. It should also be mentioned that not all the supports that were seeded were pre-treated with a surface ligand, but for those that were, the procedure is as follows.

One per cent (1%) pH neutralised 1,2-Amino–triethoxy-silane (APTES) solution was prepared prior to the surface activation process by dissolving 1ml of APTES in 100ml of distilled water. Due to the basic nature of the APTES solution, the pH of the solution is stabilised in a pH range of 6.5-7.5 using HCl under continuous stirring while constantly monitoring the pH level. The support was submerged in the APTES bath at a temperature of 90°C for 15 minutes. The support was then subsequently removed from the bath and dried at 95°C for 15 minutes. After the support had dried, it was ready for activation. Fig 3.4 shows an outline of the procedure followed in the pre-seeding treatment employed.

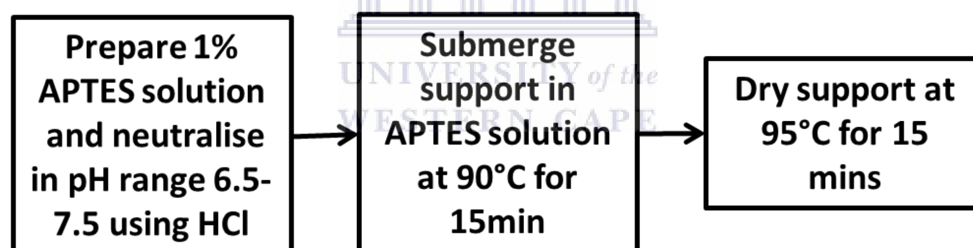

Figure 3.4: Schematic of the procedure for pre-seeding treatment

3.4 Plating

The plating procedure is the same for all samples and was carried out after the support had been properly activated. The plating bath solution was prepared in two stages with Palladium (II) Chloride ($PdCl_2$) used as the Pd precursor. The first part of the solution was prepared by dissolving 2g of $PdCl_2$ and 4ml of HCl in 200ml of distilled water. The second part of the solution was prepared by dissolving 27g Ammonia Chloride and 30g of disodium

UNIVERSITY of the WESTERN CAPE

ethylene-diamine-terta-acetic acid (Na_2EDTA) in 160ml of Ammonia hydroxide (NH_4-OH). The first solution is then added to second one and topped up with roughly 600ml of distilled water, to obtain 1L of plating solution. The solution was also mixed at a temperature of about 50°C for 30 minutes to ensure that all salts have dissolved properly. The reducing agent, N_2H_4, is also a constituent of the plating bath, but it was kept separate in order to prolong the life expectancy of the plating solution. The reducing agent was only added to the plating solution once the plating procedure was ready to commence. Details of the plating bath are shown in table 3.5.

Table 3.5: Composition of the plating bath solution

Plating bath Solution	
$PdCl_2$	2g/L
HCl (37%)	4ml/L
NH_4-Cl	27g/L
NH_4-OH	160ml/L
Na2EDTA	30g/L
N_2H_4	10ml/L
Temperature	60˚C
Duration	15 mins

UNIVERSITY of the WESTERN CAPE

Before plating, the solution was heated to 60°C. The reducing agent was added once the seeded support was completely submerged in the plating solution. The solution was continuously stirred during the plating procedure, to ensure sufficient Pd ion transfer to the solid-liquid interface during the plating procedure. In order to study the initial film microstructure, the plating process was only carried out for 15 minutes. For the fabrication of membranes for permeance testing, the plating procedure was carried out at various time

intervals. Fig 3.5 shows an outline of the procedure followed for the plating procedure employed.

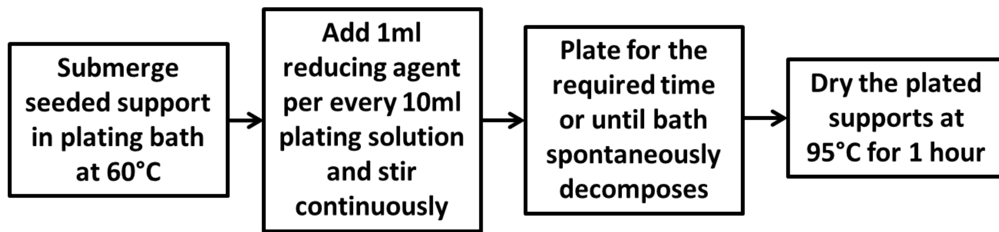

Figure 3.5: Schematic of the plating procedure

UNIVERSITY of the
WESTERN CAPE

Chapter 4: Characterisation Techniques

4.1 Scanning Electron Microscopy

4.1.1 Introduction to Scanning Electron Microscopy

Scanning electron microscopy is a technique primarily used to study the surface or near surface structure of bulk specimens [25, 26]. The scanning electron microscope (SEM) instrument makes use of a focused beam of high energy electrons (1-30KeV) [25] that strike the specimen. Electrons ejected from the surface and near surface of the specimen are then used to form high resolution image of the surface. The advantage of this technique is that it offers good spatial resolution and has a large depth of field (DOF). The following section focuses on the theory of SEM with respect to the components of the microscope and their respective functions. Image formation will also be discussed.

UNIVERSITY of the
WESTERN CAPE

4.1.2 Components of the SEM and their functions

The SEM is a complex piece of equipment; hence the exact build of one microscope is different from the other due to variation in the capabilities of each machine. However each SEM consists of similar components thus their operation is all the same. A typical SEM column is shown in Fig 4.1, and it consists of the following main components: A gun assembly, electromagnetic lenses, vacuum systems, a specimen stage and detectors.

4.1.2.1 Gun Assembly

At the very top of every SEM column is the gun assembly. This part of the microscope houses the electron source, and it is where the primary beam is produced [25, 26]. The main purpose of the gun assembly is to produce a monochromatic beam of electrons [25].

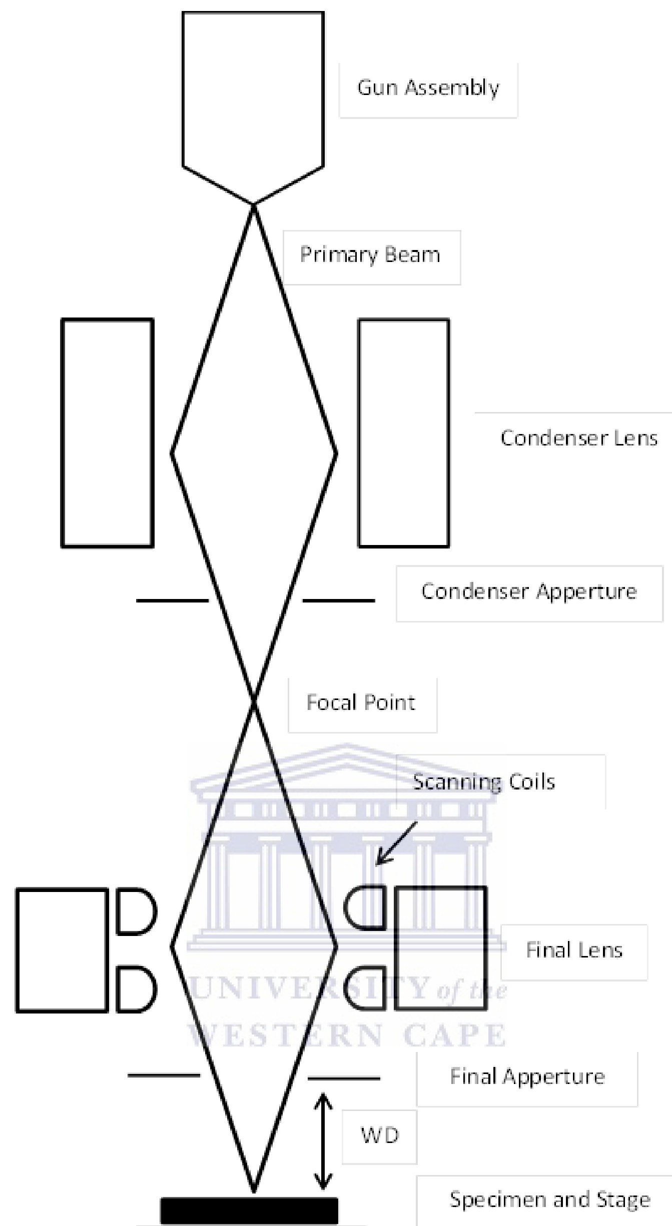

Figure 4.1: Schematic of a basic SEM Colum

There are two types of gun assemblies; namely thermionic gun, and field emission gun (FEG) [25, 26]. The former is often found in older instruments, whilst the latter is now a more common source due to its higher resolution capability [25]. As the name suggests, thermionic sources emit electrons due to heating of the filament. In FEG sources the electrons are extracted from the tip of the source by using an electric field. The resolution is enhanced in FEG electron sources as the tip of the source is very fine [25], and results in an

even more narrow spread of electrons from the source when compared to thermionic sources. This results in a smaller probe size and higher resolution.

4.1.2.2 Lens Assembly

Since the microscope makes use of electrons, which are charged particles, the lens systems in the microscope are electromagnetic [25, 26]. Through the use of electromagnetic lenses the path of an electron as it moves through the microscope column can be altered using magnetic fields. The main purpose of the lens assembly is to converge the beam, thus producing a fine beam of electrons incident on the specimen [25].These lenses are enclosed wire coils which produce a magnetic field when a current is passed through them [26]. Another part of each set of lenses is the aperture. An aperture is a small grating situated below the lenses that allows or restricts the path of the electrons through the column.

UNIVERSITY of the
WESTERN CAPE

The first set of lenses situated below the gun assembly, is known as the condenser lens. The purpose of the condenser lens is to converge the beam to a focal point below the condenser aperture. [25]. The convergence of the beam is caused by the Lorentz Force, which deflect the electrons as they pass through the lens assembly. When an electron moving with a velocity **v**, interacts with a magnetic field of strength **B**, it is accelerated by a force (**F**) given by:

$$\boldsymbol{F} = e(\boldsymbol{B} \times \boldsymbol{v}) \tag{4.1}$$

The force experienced by the electron as it travels through the column is thus perpendicular to both the magnetic field and the direction of motion of the electron. The strength of the magnetic field can be varied by changing the current in the coils of the lenses. This affects the strength of the force experienced by the electrons, which allows for the vertical variation of the focal point in the column [25].

The condenser lens converges the beam to a small spot size (2-10nm) as it hits the sample [25]. The condenser aperture is used to control the convergence angle. This is done by blocking/excluding electrons that deviate largely from the optical axes [25, 26]. This exclusion of "stray" electrons affects the image as these electrons no longer forms part of the primary beam thereby minimizing spherical aberration. This reduces the overall image brightness. As the beam converges at the focal point, it starts to spread again upon entering the final lens assembly. The purpose of the final lens is to converge the beam to a focal point on the surface of the specimen [26]. The stigmator also forms part of the lens assembly. The stigmator is used to reduce the effects of astigmatism, i.e blurriness in the image, by controlling the electron beam profile which should be circular when it reaches the specimen. The last section of the lens assembly is a set of scanning coils. The scanning coils are used to deflect the primary beam of electrons across the sample surface [26]. This scanning mechanism (rastering) is obtained by varying the current, strength of the magnetic field, in the coils.

UNIVERSITY of the
WESTERN CAPE

4.1.2.3 Vacuum systems

The use of a vacuum system is essential to any electron microscope. Since the primary beam consists of electrons, the purpose of the vacuum system is to ensure that the electrons can indeed travel through the column unhindered. The vacuum system is employed to increase the mean free path (MFP) of the electrons [26]. The MFP by definition is the distance an electron travels before colliding with air molecules. Thus through the use of a vacuum system, the MFP can be increased to be longer than the length of the SEM column. The vacuum has an additional purpose in preventing the oxidation of the electron source.

4.1.2.4 Specimen stage and detectors

The specimen stage is located below the final lens. The secondary electron detector used in image formation is situated above the stage. The distance between the stage and the final lens aperture is known as the working distance (WD) [25, 26]. Since the height and position, of the stage can be varied, the depth of focus can easily be enhanced by increasing the WD. Depth of focus is defined as the zone over which the specimen appears to be acceptably in focus [26]. To be acceptably in focus means the range in which the eye can detect no change in the sharpness of the image.

4.1.3 Image formation in SEM

When the primary electron beam strikes the specimen, it creates a volume of primary excitation as shown in Fig. 4.2 [25, 26]. From the interaction of the electron beam with the specimen, a wide range of secondary signals are produced. Scattered electrons and radiation are produced from the whole volume, but can only be detected if they escape from the surface of the specimen [25].

UNIVERSITY of the
WESTERN CAPE

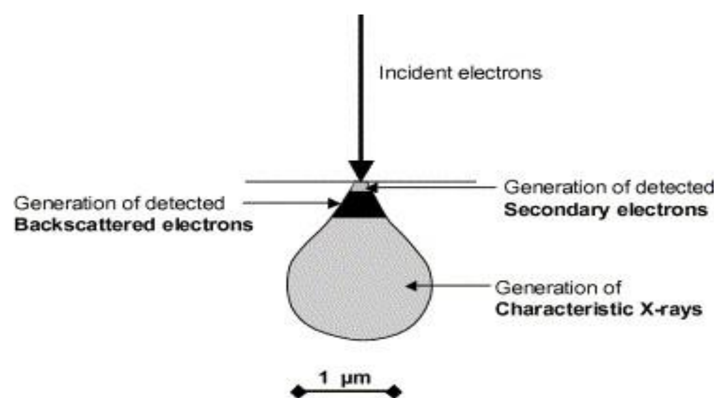

Figure 4.2: Cross sectional schematic of the primary excitation volume [26]

Two types of scattering occur within the primary excitation volume, namely elastic and inelastic scattering [26]. Elastically scattered electrons retain almost all the energy of the

primary beam; these are referred to as backscattered electrons (BE) [26]. Inelastically scattered electrons loose most of their energy and emerge from the surface of the specimen with a remaining energy in the range of 10-50 eV [25, 26]. These electrons are referred to as Secondary electrons (SE). SE are created within the complete volume of primary excitation. Most of the SE are absorbed by the surrounding atoms in the specimen due to their low energies [26]. It is for this reason that only SE near the surface of the specimen are able to escape. Since the BE are much higher in energy, they are able to escape from greater depths, up to 1 µm within the primary excitation volume [25, 26] depending on the accelerating voltage and the average atomic number (Z) of the specimen material. The sampling volume for BE signals are shown in Fig. 4.2.

UNIVERSITY of the
WESTERN CAPE

Among the other radiation types formed in the primary excitation volume are X-rays, which are of great importance. Like in the case other signals, in order for X-rays to be detected they need to escape from the specimen surface. Due to the high energies carried by the X-rays, they are not easily absorbed and most will escape. X-rays are primarily used for elemental analysis of the specimen [25, 26]. Elemental analysis is made possible due to the fact that the energy possessed by an X-ray from a specific element, is discrete. This implies that the identification of X-rays, either its wavelength or energy, from a specimen is exact to its composition. Sampling volume of X-rays is of the same order as the primary interaction volume [25]. X-rays are formed due to the process by which atoms stabilise themselves after ionisation by the primary beam [25]. The energy of the X-rays is related to the initial and final states of the transitional electron. The technique used for the detection of X-ray energies in compositional analysis is known as Electron Dispersive Spectroscopy (EDS). This is discussed in Section 4.2.7

SE are mostly used in SEM image formation. The brightness seen on the viewing screen is related to the number of SE emitted from that area of the specimen. This is referred to as amplitude contrast [26]. Amplitude contrast is controlled by two factors. The first is SE emission which is related to the composition of the specimen [26]. The second factor is the paths travelled by the SE to the detector, which is associated with the topography of the specimen [26]. With the detector situated near the sample surface, a positive bias is applied to the secondary electron detector to attract the slow moving SE towards it [25, 26]. Image formation also consists of some BE contribution [25, 26]. However this contribution is minimal, as only the BE whose paths coincide with the location of the detector, i.e. face the detector, will form part of the image [26]. Most of the faster moving BE are unaffected by the detectors bias due to their higher energies.

SE emission is partly dependant on the specimen's composition i.e. greater atomic number (Z) means more SE generation [26]. This is due to the increased electron density of the heavier elements. The effect of topography on image formation is a result of the detector location [26]. If we consider a specimen with a peak in the middle, we find that SE generated from areas of the specimen facing the detector, would reach the detector unobscured. SE generated from areas facing away from the detector will thus have their paths obscured by the peak in the centre. The obstruction of the SE signal by the peak causes a shadowing effect i.e. due to the placement of the detector on one side it makes it seem as if a light is shining on the specimen from one side [26]. Peak tips i.e. thinner areas emit SE more efficiently, and we find that finer structures appear brighter in the image [26]. To negate the effects of topography the specimen can be tilted, thus improving the paths the electrons follow to reach the detector and maximising signal detection.

UNIVERSITY of the
WESTERN CAPE

With the use of the scanning coils, the beam is deflected over the sample surface. SE as well as some BE are collected from the desired specimen area, which results in the formation of an SE image. [26]. BE signal can also be used to form images, although this is not a common practice nowadays as SE signal is the most preferred method for image formation [25, 26]. Increased BE signal is obtainable through the removal of the detector bias. Similarly to the case of a SE image, only few SE electrons facing the detector contribute to BE image formation [25, 26].

4.1.4 Sample preparation for SEM characterisation

Surface characterisation of the samples was done using the high resolution (HR) Auriga Field Emission SEM. In preparation for characterisation, samples were mounted onto SEM specimen stubs using either carbon or copper tape with no further modifications. During analysis SEM micrographs were obtained at WD of roughly 5mm. To reduce the effects of charging on the samples, accelerating voltages were kept fairly low at 5kV. During EDS analysis the accelerating voltage was increased to 10kV to ensure that the beam was energetic enough to generate Pd signals (see section 4.2.7). -

UNIVERSITY of the
WESTERN CAPE

4.2 Transmission Electron Microscopy

4.2.1 Introduction to Transmission Electron Microscopy

The TEM is superior to SEM in its ability to obtain higher resolution. This is due to the initial energy obtained by the electron, which is about 10 times that of an electron in SEM. Typical accelerating voltages for TEM is around 100-300 kV [25, 26].

$$r = \frac{0.61\lambda}{\alpha} \quad (4.2)$$

$$\lambda = [\frac{1.5}{(V+10^{-6}V^2)}]^{1/2} \text{ [nm]} \quad (4.3)$$

Equation 4.2 gives the relationship between resolution (r) and the wavelength (λ) for the electrons. This is an adaptation of Abbe's equation for small converging angles (α). A smaller r value indicates higher resolution as it determines the smallest distance between two entities at which they appear to be completely resolved. The dependence of the electron wavelength to the accelerating voltage (V) is also shown in the equation 4.3. This expression is derived from the de Brogile relationship, as well as taking into account relativistic effects. At high accelerating voltages we find that the velocity of the electron is a significant fraction of the speed of light. This results in short wavelengths, which in-turn results in enhanced resolution.

TEM images are formed by contrast effects given by electrons transmitted through the specimen. It is for this reason that TEM specimens have to be very thin (roughly 10nm thick) to allow for electron transmission. Since these transmitted electrons are used in imaging, TEM is used to study the internal structure of the specimen [25].

UNIVERSITY of the
WESTERN CAPE

The theory of TEM is similar to that of SEM in many ways. The basic construction of the microscope column is similar to a SEM with only a few differences. Fig. 4.3 shows a schematic of a basic TEM column. In the following sections, the theory of transmission electron microscopy will often be discussed in reference to that of scanning electron microscopy. Sections 4.2.2 and 4.2.3 describe the theory and image formation of TEM respectively.

4.2.2 Components of the TEM and their functions

The very top part of the microscope column, shown in Fig. 4.3, is home to the gun assembly. Similarly to SEM instrument, the electron source in TEM is either thermionic or a FEG [25]. FEG sources, in TEM, are more commonly used due to its production of a very fine

spread (about 1nm) of electrons in the primary beam [25]. As in SEM all the lenses in TEM are also electromagnetic the condenser system is also located just below the gun assembly. This usually consists of two or more lenses separated by an aperture [25]. As in SEM the first set condenser lenses converges the primary beam of electrons, and the aperture controls the diameter of the beam by varying the convergence angle [25]. The beam is then made to converge to a focal point on the specimen by the second set of condenser lenses [25, 26].

The specimen chamber in TEM is actually positioned between the objective lens just above the objective aperture [25]. The purpose of the objective lens is twofold. It is responsible for the formation of the first intermediate image of the specimen as well as the image of the diffraction pattern [25]. It should be noted that both the imaging and diffraction modes cannot be in operation at the same time. The instrument operator is able to switch between the two as desired [25].

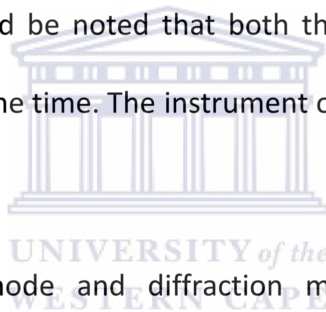
UNIVERSITY of the
WESTERN CAPE

The switch between image mode and diffraction mode is controlled by the first intermediate lens. Some instruments employ more than one intermediate lens. When in imaging mode, the first intermediate lens focuses on the image plane of the objective lens [25]. This results in a viewable image of the specimen on the viewing screen. When in diffraction mode, the intermediate lens is set to focus on the back focal plane of

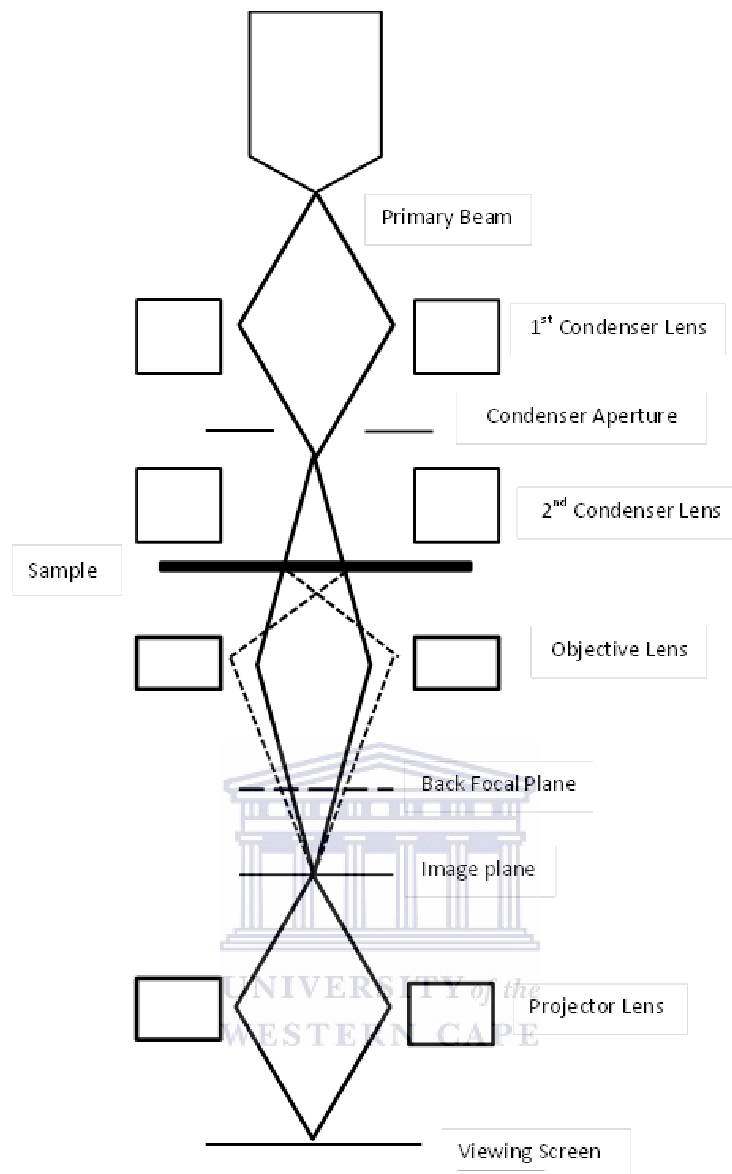

Figure 4.3: Schematic of a basic TEM column

the objective lens [25]. A diffraction pattern is then observed on the viewing screen. The final magnification of both the image and diffraction patterns on the viewing screen is controlled by the final set of lenses known as the projector lens [25].

Vacuum systems are also required in the TEM. Generally the vacuum in TEM needs to be higher than in SEM as the TEM microscope column is longer. This higher vacuum ensures the extension of the MFP of the electrons which need to reach the detector at the bottom of the column.

4.2.3 Contrast mechanisms and image formation in TEM

Only electrons that are transmitted through the specimen, and pass through the objective aperture will contribute to the image on the viewing screen [25]. Image contrast is also formed by those electrons that do not reach the detector due to high angle scattering. The objective aperture, located in the back focal plane of the objective lens, defines the angular range of electrons in the transmitted beam. It is the transmitted electrons which contribute to the nature of contrast formed in the mage [25]. The size and position of the objective aperture controls the type of contrast evident in the image [25].

UNIVERSITY of the
WESTERN CAPE

Most common imaging mode used in TEM is known as bright field imaging. This is when the objective aperture is centred about the optical axis. In the absence of a specimen no electrons are scattered, and a bright background is seen on the viewing screen. Thus regions of the specimen which are thick or have a high density, will scatter electrons strongly, and appear dark on the image as these electrons do not pass through the objective aperture. The difference in scattering events due to thickness is influenced by the path travelled through the specimen. In a thicker area an electron is more likely to encounter an atom to scatter from, when compared to a thinner area. Hence scattering is more probable in thicker sites of the specimen [25].

The contrast due to density is explained in a similar manner as above for thickness contrast. More scattering will occur in the more dense areas than in the less dense ones [25]. The

probability of scattering in the more dense area is higher, due to the higher number of atoms in that region. As the beam passes through the specimen it is scattered strongly in the denser area, hence these electrons do not pass through the objective aperture. This results in darker contrast for that region on the image [25].

4.2.4 Sample preparation for TEM characterisation

The instrument used in this study for TEM characterisation is the Technai G^2 F20 X-Twin MAT 200 kV Field Emission TEM. In preparation for TEM analysis, the surface of the various fabricated samples was scratched onto glass slides to dislodge the samples constituents. Ethanol was added to the sample residue, and holey carbon 200 mesh TEM grids were dipped into the solutions containing the sample residue. The grids were then air dried overnight, before analysis.

UNIVERSITY of the
WESTERN CAPE

4.2.5 Electron Diffraction

4.2.5.1 Introduction

Fig. 4.4 shows a schematic of electron scattering within a thin perfect cubic lattice.

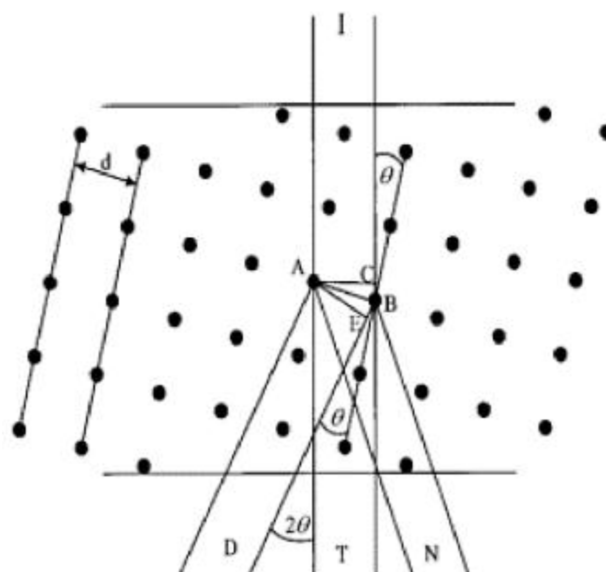

Figure 4.4: Scattering of an incident beam of electrons [25]

A beam of electrons incident on the sample, indicated by I, will be elastically scattered by the atoms A and B in the specimen. The beam of electrons at I are coherent i.e. each electron wave is in phase and thus constructively interfere which results in a strong reinforced beam of electrons [25]. If theses waves are out of phase they will interfere destructively [25]. From the image the beam of electrons at point T pass through the specimen undeflected. At point D the beam has been diffracted whilst at N no intense beam is formed due to destructive interference. The scattered waves at D are in phase if their paths lengths differ by an integral number of wavelengths shown in equation 4.4, where n is an integer and λ is the wavelength of the electrons [25].

$$CB + BE = n\lambda \qquad (4.4)$$

From Fig. 4.4 using simple geometry BE = CB = d sinθ. This means that the requirement for coherency is given by equation 4.5.

UNIVERSITY of the
WESTERN CAPE

$$2d \sin\theta = n\lambda \qquad (4.5)$$

This equation 4.5 is well-known as Braggs law, and is applied to the diffraction of x-rays and electrons. The interplanar spacing between planes of atoms is denoted by d, n is the order of diffraction and θ is the angle of incidence of the electrons on the plane of atoms. This law tells us that electrons will only be elastically scattered if they are at an angle θ which is a solution to equation 4.5 [25].

The inter-planar spacing d is determined by the standard Miller index notation. For a cubic crystal of plane (***hkl***) the inter-planar spacing is defined by equation 4.6.

$$d = \frac{a}{(h^2+k^2+l^2)^{\frac{1}{2}}} \qquad (4.6)$$

The variable a is the unit cell length of the specimen crystal, also called the lattice parameter. For electron diffraction it is convenient to consider only first order diffraction, i.e. n=1 in equation 4.5 [25]. Due to the high energy, i.e. short wavelength (λ), of the electrons, typical scattering occurs at very small angles, and by the small angle approximation the equation can be simplified further. Strong diffraction of electrons thus only occurs by atomic planes almost parallel to the incident beam of electrons. Bragg's law for electron diffraction is thus given by equation 4.7.

$$2d\theta = \lambda \quad (4.7)$$

4.2.5.2 Diffraction in TEM

In TEM two types of images can be formed from the specimen, namely a magnified image, as well as a diffraction pattern [25]. A diffraction pattern of the specimen can be seen when the viewing screen is placed in the back focal plane [25]. The formation of these images can be explained in terms of simple geometry given in Fig. 4.5.

UNIVERSITY of the
WESTERN CAPE

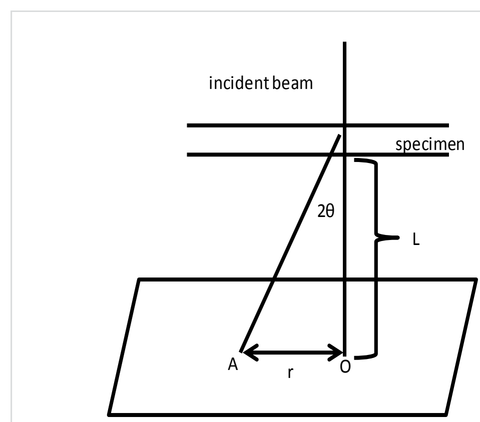

Figure 4.5: Schematic representation of diffraction in TEM

For a beam of electrons incident on a crystalline specimen, some of the electrons pass through it and arrive on the viewing screen at point O**.** For the electrons that get diffracted

at an angle 2θ, they arrive at the viewing screen at point A some distance r away from point O. The distance from the specimen to the viewing screen is given by L. From the geometry it is easy to see that rL = tan 2θ. Since θ is very small tan2θ = θ. When this equation is combined with Braggs law for electron diffraction, equation 4.7, we arrive at the relation given below.

$$\frac{r}{L} = \frac{\lambda}{d} \; ; \; rd = \lambda L \quad (4.8)$$

The product λL is known as the camera constant, as both λ and L are independent of specimen and fixed for the instrument being used. The relation above shows that the distance of the diffracted spot r is thus inversely proportional to the inter-planar spacing of the atomic planes that cause diffraction. If we know the camera constant we can easily determine the value of d by simply measuring r on the diffraction pattern.

If we consider a single crystalline specimen then several sets of planes are thus parallel to the incident electron beam. This results in a diffraction image that is a pattern of regular array of spots [25]. For a multigrain specimen, i.e. those that have atomic planes of different orientations, only certain planes that satisfy the Bragg condition will diffract incoming electrons. This results in diffraction image of a pattern of spots that fall on rings, of which each ring has a constant r [25]. For a poly-crystalline sample, i.e. a sample consisting of many crystals of random orientations, the spots on the rings are very close. The diffraction observed in this instance is thus a continuous ring pattern [25].

UNIVERSITY of the
WESTERN CAPE

4.2.6 Scanning Transmission Electron Microscopy

Scanning coils are required to operate the instrument in this mode of imaging. When the machine is operated in scanning transmission electron microscopy (STEM) mode, a high

angle annular dark field (HAADF) detector is inserted below the specimen. This detector collects the electrons that have been scattered through large angles. Since inelastic scattering power is greatly affected by the atomic number (Z) of the specimen, STEM is powerful in imaging specimens that have complex structures i.e. alloys [25]. The greater the atomic number of the area on the specimen, the brighter the contrast at that point of the image.

4.2.7 Energy Dispersive Spectroscopy

4.2.7.1 Introduction

Energy dispersive spectroscopy (EDS) involves the analysis of X-ray energies. The interaction of the primary beam with atoms in the specimen causes the formation of vacancies in the shells of the atoms due to scattering. These vacancies are then filled by electrons from another shell of the same atom, and releases X-rays. From the Bohr model of the atom, it is evident that these shells are found at discrete levels, and thus the energy of the released x-rays is also discrete. It is for this reason that X-rays are used for elemental analysis of specimens in both SEM and TEM.

UNIVERSITY of the
WESTERN CAPE

4.2.7.2 Electron dispersive spectrophotometers

Since X-rays carry no charge their paths cannot be influenced in any manner. Electron dispersive spectrophotometers thus need to be situated near the specimen to maximise the collection of x-rays from the specimen [25]. Most common type of detector used in EDS is a Silicon-Lithium (SiLi) semiconductor detector [25, 26]. Each x-ray that enters the detector excites numerous electrons from the valance band (VB) to the conduction band (CB) of the semiconductor. This excitation creates a number of electron-hole pairs [25]. For the SiLi detector each excitation is about 3.8 eV so that an x-ray of 3.8 keV would create 1000

excitations. As x-rays are absorbed, voltage is applied across the semiconductor which causes a pulse of current proportional to the x-ray energy to flow [25]. This created pulse is then amplified and passed to a multi-channel analyser (MCA) which registers the x-ray in a specific channel according to its energy. Each channel within the MCA represents different x-ray energies and the MCA is able to collect a histogram of energies, which it then displayed on the computer screen [25].

In the SiLi detector setup, elements lighter than berrylium (Be) cannot be detected [25]. SiLi detectors are also very efficient as almost all incoming x-rays produce pulses. The processing of pulses takes time as they need to be amplified and sorted. This implies that a second pulse cannot be detected until the first pulse has been completely processed. Total time elapsed during analysis is the sum of the live time and the dead time. Live time is defined as the time during which the detector is counting pulses, with the dead time defined as the time the detector ignored incoming x-rays due to signal processing.

UNIVERSITY of the
WESTERN CAPE

An important factor to remember when using EDS is that the energy of the generated x-rays cannot be greater than that of the primary beam [25, 26]. This should be taken into account when probing the specimen for specific elements. The most admirable property of EDS is that it allows for the collection of a complete spectrum and qualitative analysis in a few minutes [25]. This is made possible by the highly efficient detectors used in the technique.

4.3 Permeance Testing

4.3.1 H_2 permeation through Pd membranes

The steady state permeation rate, i.e H_2 flux (J), is given by the equation 4.9 [6]

$$J_H = \frac{P(p_f^n - p_p^n)}{L} \tag{4.9}$$

In equation 4.9 J_H denotes the hydrogen flux, where P is the permeability, L is the thickness of the Pd layer, p_f is the partial pressure of the feed side, i.e. the side at which H_2 enters the membrane, p_p is the partial pressure of the permeate side, i.e. the side at which H_2 exits the membrane, and n is the pressure exponent. The value of n ranges between 0.5 and 1 depending on what step in the diffusion process is the rate determining step [1, 6]. The permeability (P) of H_2 through a metal is a function of diffusivity (D) and solubility (S) as shown in equation 4.10 [6].

$$P = S \cdot D \tag{4.10}$$

Diffusion of H_2 through the Pd membranes occurs as a result of the difference in partial pressure across the metal [6]. The mechanism of H_2 permeation through Pd membranes is what is termed a solution-diffusion mechanism [1, 6] and proceeds as follows.

1. H_2 molecules diffuse through the boundary layer formed at the gas solid interface
2. The diatomic H_2 is chemisorbed absorbs onto the metal surface and dissociates into atomic H atoms
3. H atoms are absorbed into the bulk Pd layer
4. H atoms diffuse through the metal to the opposite surface
5. Recombination of the atomic H into diatomic H_2 occurs at the opposite surface
6. The H_2 then diffuses away from the surface

UNIVERSITY of the
WESTERN CAPE

Equation 4.11 shows the chemical formula for the dissociation and recombination of H_2 as it diffuses into and out of the Pd membrane [6].

$$H_2 \leftrightarrow 2H \tag{4.11}$$

Assuming equilibrium between H_2 in the gas phase and the atomic H in the metal, the concentration of atomic H (c_H) in the metal is given by Sieverts Law shown in equation 4.12.

$$c_H = K_s p_H^n \tag{4.12}$$

Sieverts constant (K_s) describes the solubility of the atomic H in the metal, and p_H denotes the partial pressure of H_2 in the gas phase. The square root of hydrogen pressure dependence, i.e. n=0.5, is only valid in the assumption of Sieverts Law when the atomic H in the metal lattice is dilute and there is virtually no interaction between H atoms [6]. Another descriptive model should be devised if the surface conditions such as dissociation/recombination or adsorption become the rate controlling step for H_2 permeation through the metal.

Deviations from the half-power pressure dependency diffusion system include defects, i.e. cracks or pin holes, which are found in the membrane. The defects found in membranes lead to Knudsen diffusion [6]. Knudsen diffusion is when the mean free path of an atom/molecule is greater than the pore diameter of the membrane [6]. This implies that pore wall collisions occur more frequently than intermolecular collisions. Knudsen diffusion thus contributes largely to the total diffusion in the membrane, and is thus not favourable in gas separation [6].

UNIVERSITY of the
WESTERN CAPE

Other deviations from the half-power pressure dependency diffusion system include, changes in the structure of the film, i.e. α/β phase transformations, contamination and thermal stresses that are caused by large differences in the linear thermal expansion co-efficient between the Pd film and support [1, 6]. All these factors mentioned influence the gasses ability to diffuse through the metal lattice.

4.3.2 Gas permeation tests

In order to determine the quality of the fabricated membranes, each of the fabricated samples were subjected to single gas permeation tests of both H_2 and N_2 gasses. Fig. 4.6 (left) and (right) shows the schematics of the module and experimental setup used for permeation tests respectively.

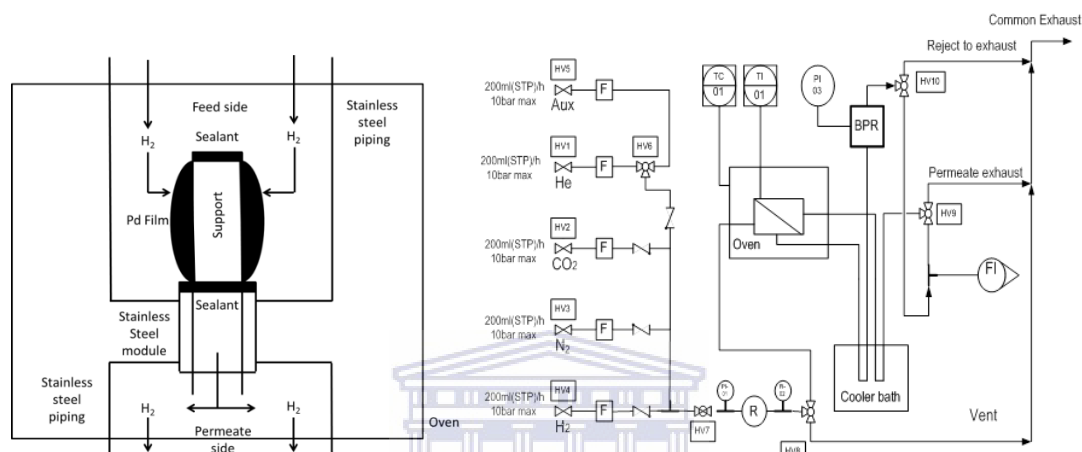

Figure 4.6: Schematics of the membrane module situated in the oven (left) and permeation test station (right)

UNIVERSITY of the WESTERN CAPE

The module consisted of the Pd membrane with one end sealed that was placed in a stainless steel tube. The other end of the membrane was connected to the permeation station. The gap between the membrane and the stainless steel module, as well as the upper end of the membrane was sealed using Eagle Star High Temperature (340°C) Red RTV Silicone Gasket Maker.

The suitability of the sealant was verified by testing a blank support at low temperature (25°C), and high temperature (320°). The pressure gauge monitored the pressure of the gas flowing towards the membrane, i.e. feed side, with the pressure on the permeate side being atmospheric as the gasses exits out of the flow meter after the flow is measured. The

permeability of a single gas, N_2/H_2, through the membrane was measured at room temperature and 320^oC for N_2 gas and measured only at 320^oC for H_2 gas.

Chapter 5: Results and Discussion

In this chapter, the results for seeded supports, plated supports, as well as the permeance tests for the different supported membranes are presented and discussed. In section 5.1 and 5.2 the SEM and TEM results of seeded supports respectively are presented and analysed. Section 5.3 relates to the discussion of the seeded supports. In section 5.4 SEM analyses of the plated supports are given with section 5.5 relating to the discussion of the results obtained from the plated supports. Section 5.6 concludes the chapter with a presentation and discussion of the permeance results.

5.1 SEM Analysis on seeded supports

For SEM analysis various alumina (i.e. ceramic) supports were seeded using the different activation, and pre-treatment methods described in section 3.3. Table 5.1 lists the methods used during activation of the samples M1-M5.

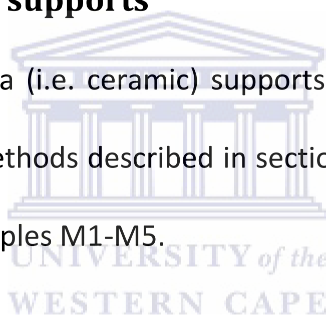
UNIVERSITY of the
WESTERN CAPE

Table 5.1: List of all the seeded supports fabricated in this study

Membrane	**Procedure**			
Name	**APTES**	**Method 1 (N_2H_4)**	**Method 2 (H_2)**	**Method 3 ($SnCl_2$)**
M1	**X**	**X**		
M2	**X**		**X**	
M3		**X**		
M4			**X**	
M5				**X**

Supports activated by pre-treatment with APTES and reduced using dilute N_2H_4 are referred to as M1. Supports activated by pre-treatment with APTES and reduced using H_2 gas are referred to as M2. Samples M3 and M4 were reduced by dilute N_2H_4 and H_2 gas respectively, without any support pre-treatment. Finally sample M5 denotes the support activated using a conventional Sn based reduction method.

During SEM analysis multiple areas of each the sample were probed and images used in this section are found to be representative of the whole sample. Fig. 5.1 (a) and (b) shows the SEM micrographs of seeded supports M1 and M3. As mentioned in table 5.1 M1 differs from M3, as it was subjected to a surface pre-treatment with APTES.

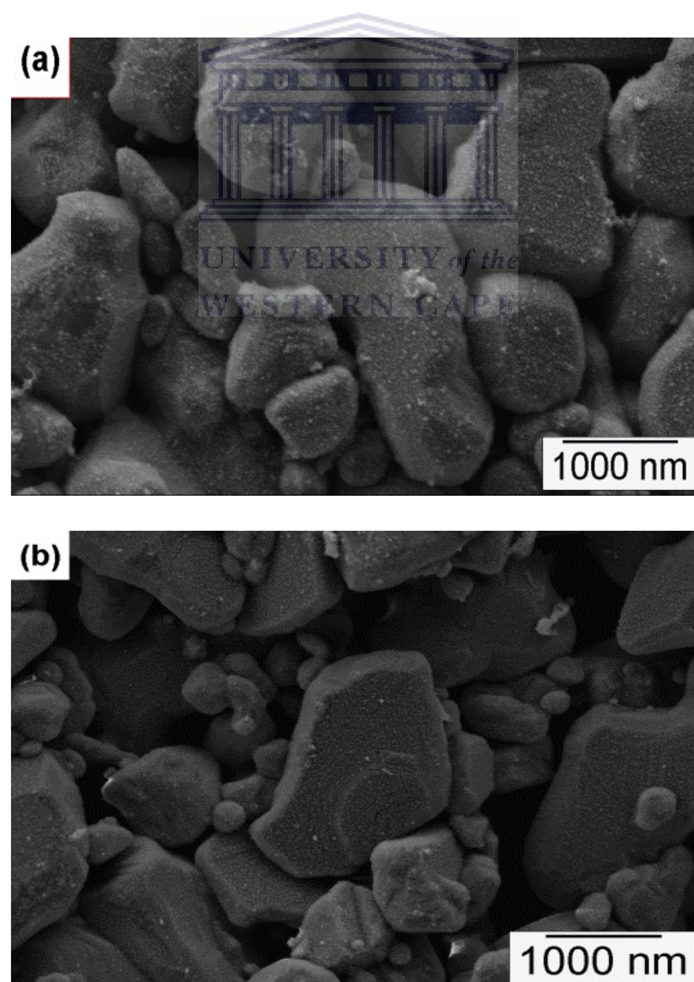

UNIVERSITY of the
WESTERN CAPE

Figure 5.1: SE images of seeded supports (a) M1, and (b) M3

For both M1 and M3 the supports were seeded until proper activation was achieved. This required repeating the seeding procedure an average of 7 times. The supports of both M1 and M2 appear to be uniformly covered in tiny seeds which appear on the image as light grey dots. In Fig. 5.1 it appears that seed coverage for M1 is greater than in M3 as the surface appears to be covered in a sort of "fluff". Coverage is also better when considering the levels of contrast in the images which appears to be higher in the image of M1 than in the image of M2.

Fig.5.2 (a)-(c) shows the SEM images obtained from samples of type M3 seeded once, twice and thrice respectively; Fig. 5.2 (d) displays a micrograph taken from a sample of type M1 seeded twice.

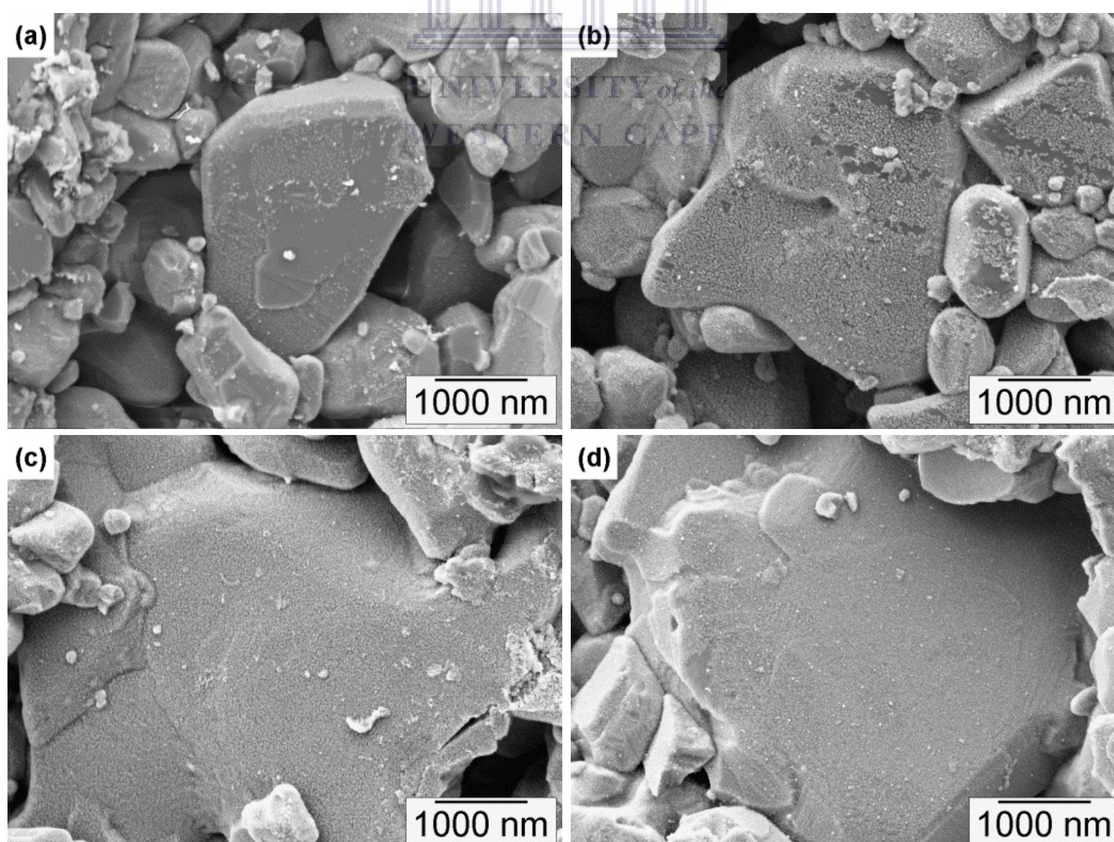

Figure 5.2: SE images for samples of type M3 seeded (a) once (b) twice (c) thrice and (d) sample of type M1 seeded twice

UNIVERSITY of the WESTERN CAPE

Table 5.2 shows the coverage obtained during progressive seeding when using dilute N_2H_4 as a reducing agent. Various areas of a fixed size were measured on flat regions of the support. Support coverage was then calculated as a percentage by measuring the seeded areas within the total fixed area. Figure 5.3 shows the plot of the data from table 5.2

Table 5.2: Coverage obtained during seeding

Sample Type	# of seed steps	Coverage (%)
M1	2	98
M3	1	19
M3	2	55
M3	3	93

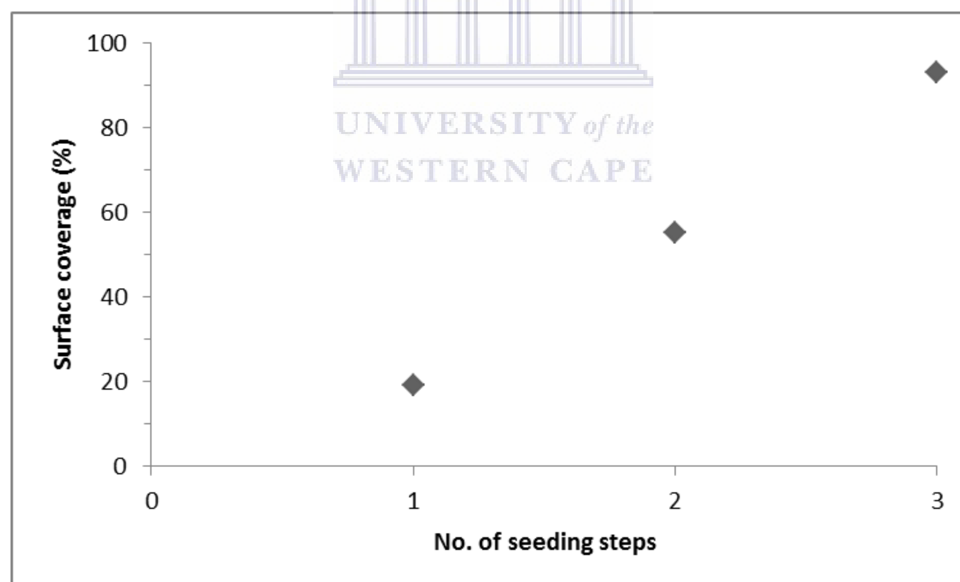

UNIVERSITY of the
WESTERN CAPE

Figure 5.3: Plot showing the increase in surface coverage for by Pd seeds with increasing number of seeding steps for M3

From the results in table 5.2 and illustrated by Fig 5.3, it was observed that with progressive seeding the seed coverage on the support increased significantly when APTES was not used

(type M3). In the once seeded sample, unseeded areas are large at around 80% of the measured areas. When a second seeding procedure is applied these unseeded area sizes decrease significantly to 45%. The size of unseeded areas for M3 only becomes comparable to that of M1 after three seeding procedures.

The SEM micrographs of seeded supports M2 and M4 are shown in Fig. 5.4 (a) and (b respectively. Both samples were seeded seven times.

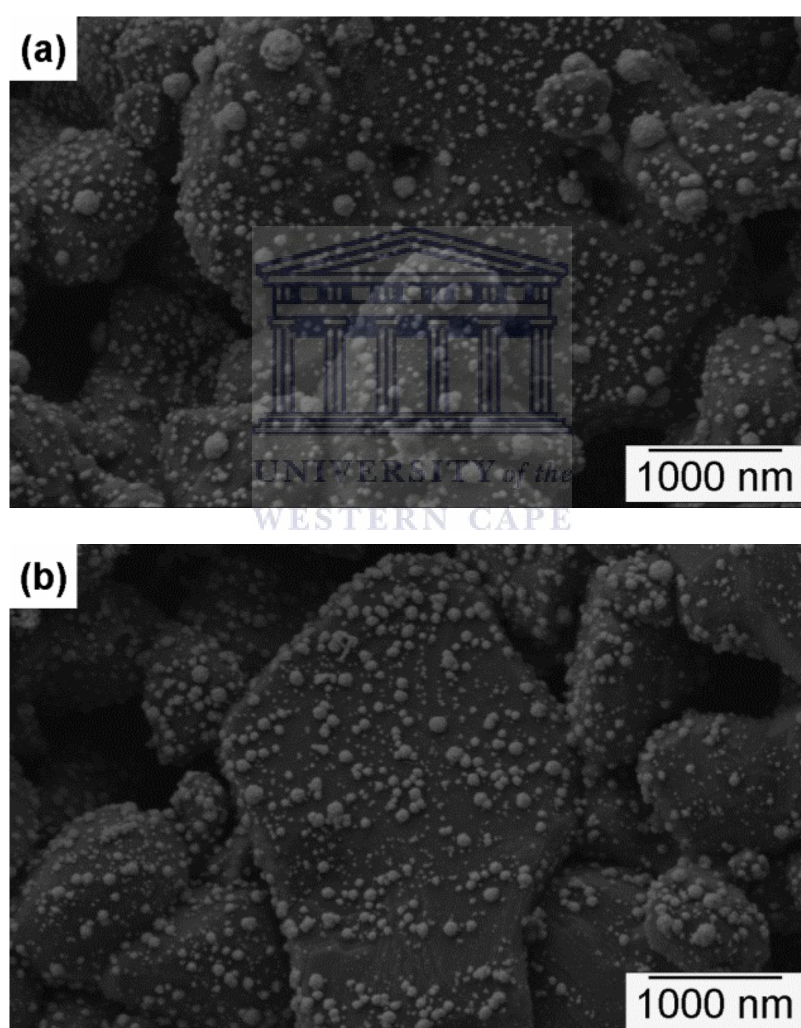

UNIVERSITY of the
WESTERN CAPE

Figure 5.4: SE images of seeded samples (a) M2, and (b) M4

In addition to H_2 gas reduction, sample M2 was also subjected to a surface pre-treatment with APTES. In contrast to samples M1 and M3, reduction via H_2 gas resulted in the

formation of larger spherical clusters on the surface of the support. Seeds are also uniformly distributed on the surface of the support, and display large particle size distributions due to possible agglomeration.

Fig 5.5 shows the plots of the particle size distributions for samples M2 and M4. The ranges of particle sizes were obtained by measuring across the longest diameter of various particles on the support surface.

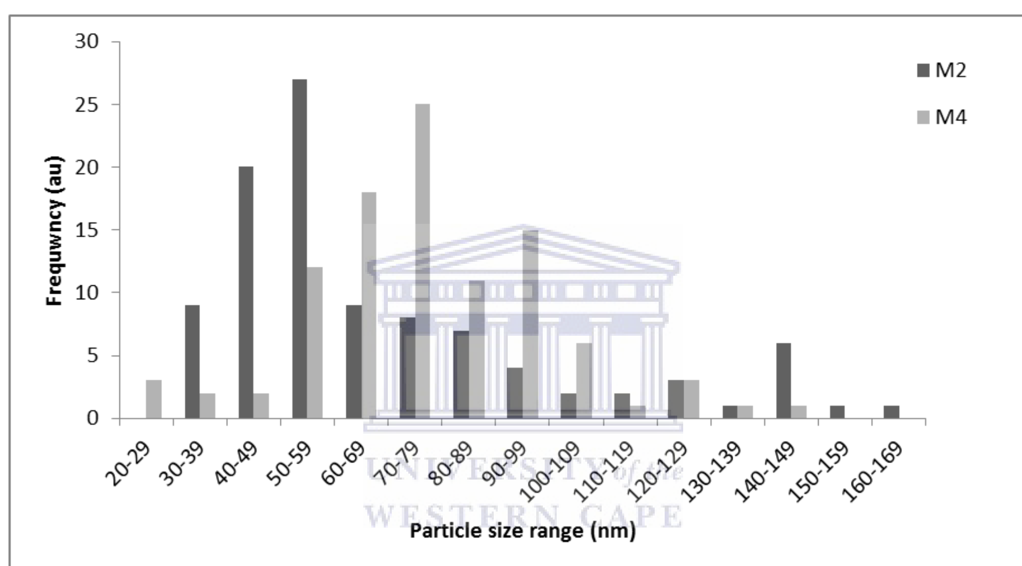

Figure 5.5: Plot showing the particle size distribution of seeds on M2 and M4

Most of the particles found on the surface of M2 are in the range of 30-99 nm. In the case of M4 most particles found on the surface are in the range 50-109nm.

Table 5.3 shows various particle size statistics obtained for M2 and M4. The average particle size for each sample shown in Table 5.3 was calculated using imageJ software. Particle sizes were calculated using the equivalent diameter measured for each seed within the defined ranges of 30-99nm for M2 and 50-109nm for M4.

Table 5.3: Particle size statistics in samples M2 and M4

Sample	Average particle size (nm)
M2	52
M4	78

Table 5.4 shows the level of seed coverage exhibited by M2 and M4.The data in table 5.4 was obtained by counting the number of particles within an area of a fixed size. All particles that coincided with the edge of the fixed area were not included in count. The average area per particle was then calculated by dividing the size of the area by the number of seed particles contained within the area.

Table 5.4: Support coverage of samples M2 and M4

Support coverage	
Sample	Average Area per particle (nm^2)
M2	6900
M4	8924

UNIVERSITY of the
WESTERN CAPE

From table 5.4 it is observed that the average area per particle is smaller for M2 than for M4. This translates into a greater level of support coverage by M2 when compared to M4.

The SEM micrographs displayed Fig 5.6 show the images taken from the surface of (a) an unseeded/blank support, and (b) a conventionally seeded support referred to as M5. Sample M5 is obtained from a standard and established method for dense Pd membrane fabrication [1, 5, 6]. It is for this reason that it will be used as a standard to which to compare the other processed samples.

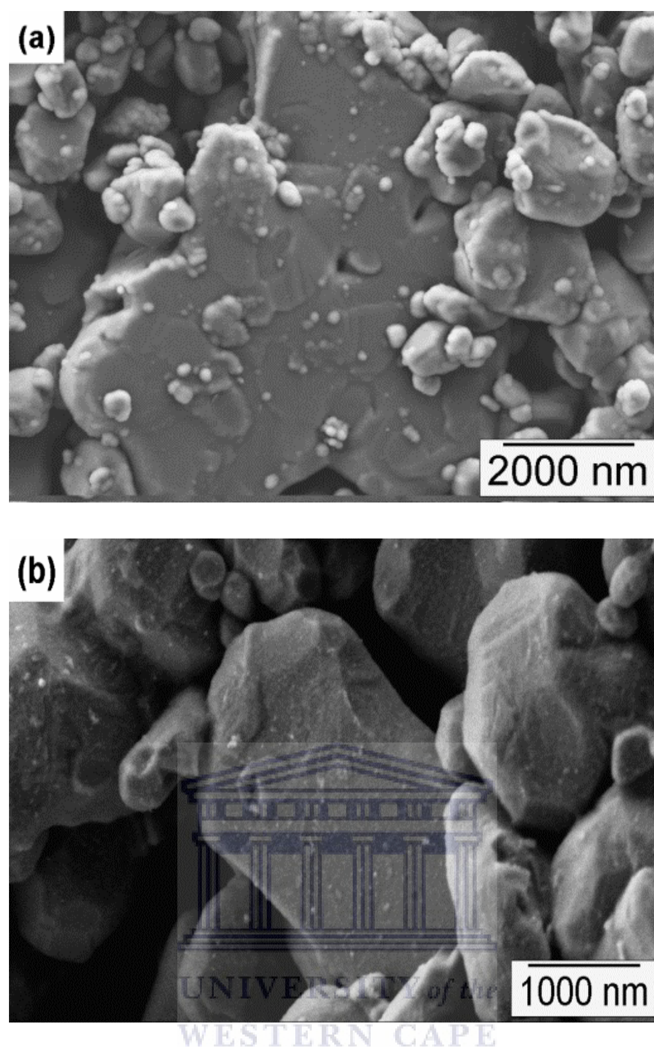

UNIVERSITY of the
WESTERN CAPE

Figure 5.6: SE images of (a) blank support and (b) sample M5

When comparing the images of the blank to M5, a modification to the support surface of M5 is observed although hardly visible. Similar to M1 and M3 the seeds are identified as the light grey dots on the support surface, this is an absent feature when looking at Fig. 5.6 (a). The seeds in M5 display uniform and complete coverage of the support.

In table 5.5 the elemental compositions obtained by EDS for various areas on sample M5 are shown.

Table 5.5: Elemental composition of various areas of sample M5

Area 1		Area 2		Area 3		Area 4	
Element	**Wt%**	**Element**	**Wt%**	**Element**	**Wt%**	**Element**	**Wt%**
O	41.24	O	44.65	O	41.3	O	37.84
Al	41.77	Al	48.48	Al	43.53	Al	38.35
Cl	0	Cl	0.58	Cl	0.7	Cl	5.2
Cu	3.61	Cu	0	Cu	0	Cu	2.98
Pd	3.53	Pd	1.37	Pd	11	Pd	10.4
Sn	9.84	Sn	4.92	Sn	3.48	Sn	5.22
Total:	100	Total:	100	Total:	100	Total:	100

Elements Al and O are the constituents of the ceramic support, whilst Cu and Cl are derived from the copper tape adhesive used to secure the sample to the stub for analysis, and the chloroform ($CHCl_3$) used during sample fabrication respectively. Table 5.5 shows that in areas 1 and 2 the amount of Sn present on M5 is more than double the amount of Pd in the same region. In the other two areas the amount of Sn ranges from about 30-50% the amount of the Pd.

UNIVERSITY of the
WESTERN CAPE

5.2 TEM Analysis on seeded supports

As explained in section 4.2.4, TEM samples were prepared by scrapping the seeded support surface with a surgical blade. The residue of each sample was then mixed with ethanol to help transfer the constituents to a copper grid for analysis.

Fig. 5.7 (a) shows a low magnification image of a piece of the support on the edge of the carbon film of the TEM grid. The Pd seeds can be seen on the support as the dark spots. Fig. 5.7 (b) offers a closer look at the distribution of the seeds on top of the support pieces. The seeds (seen as dark spots in the image) pack closely together in some areas, and in other

areas they form short chains. Seeds are mostly spherical in shape but also exhibit a hexagonal structure in some few cases. Similar shapes for Pd particles have also been reported previously [27]. SAD pattern shown in Fig. 5.7 (c) shows that the seeds formed in M1 and M3 are single crystalline and display the typical FCC structure expected from Pd. The images shown below are thus representative of both samples M1 and M3.

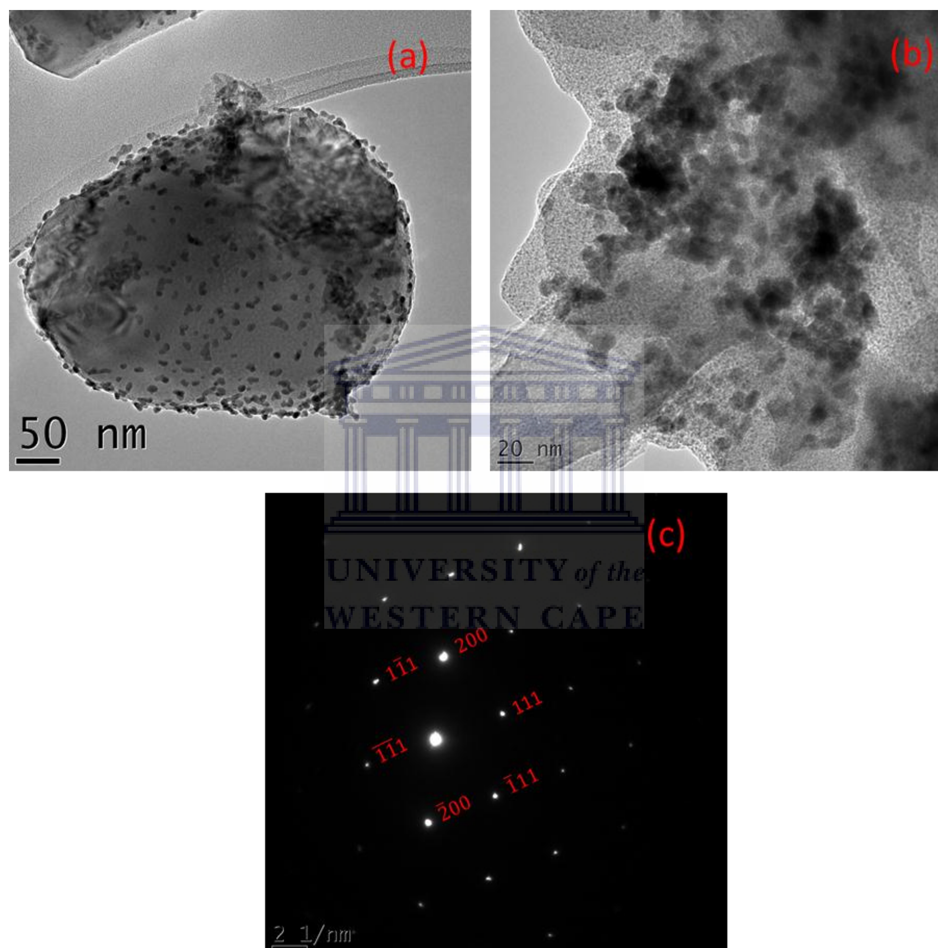

UNIVERSITY of the
WESTERN CAPE

Figure 5.7: Bright field TEM images of (a) the seeds on the support, (b) the seed distribution and (c) SAD pattern of seeds for samples M1 and M3

Table 5.6 shows the range of particle sizes exhibited by samples M1 and M3. Seed diameters were calculated by measuring across the longest diameter of multiple seeds displayed on the support surface in TEM images.

Table 5.6: Particle size ranges for samples M1 and M3

Sample	Particle size range (nm)
M1	4-7
M3	9-11

Seeds on the surface of M1 were observed to be smaller than those found on the surface of M3 as shown by the various size ranges given in Table 5.6.

Fig 5.8 shows a representative EDS spectrum for both samples M1 and M3.

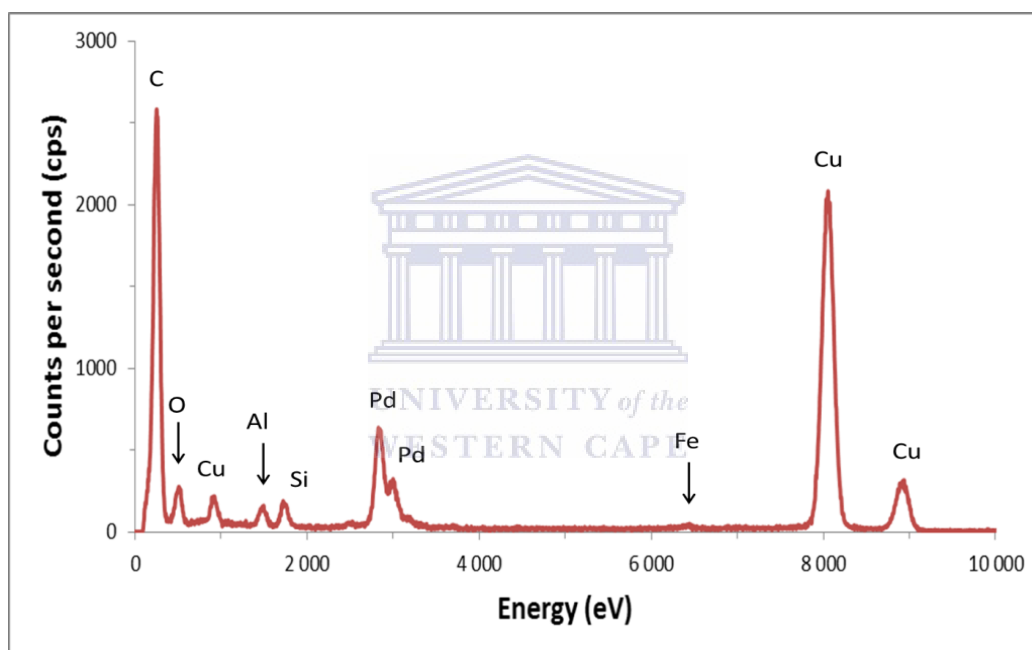

Figure 5.8: A typical EDS spectrum for samples M1 and M3

EDS spectrum shown in Fig 5.8 shows the typical elements found for both M1 and M3. Whilst the intesities of the peaks may have differed, it is the elemetal constiutents that were the same for all of the areas that were analysed. EDS confirms the presence of Pd seeds as well as elements Al and O which are constituents of the alumina support. Elements C an Cu

are derived from the TEM grid, whilst the Fe could have been present as a constituent of the blade used to scrape the seeds off of the Al_2O_3 support onto the TEM grid.

Figure 5.9 shows the TEM images and selective area diffraction (SAD) pattern obtained from samples M2 and M4. A low magnification image of pieces of the sample support is shown in Fig. 5.9 (a). A closer look of the seeds on the support is shown in Fig. 5.9 (b), whilst a SAD pattern of the Pd seeds is displayed in Fig5.9 (c). The images shown below are also representative of both samples M2 and M4.

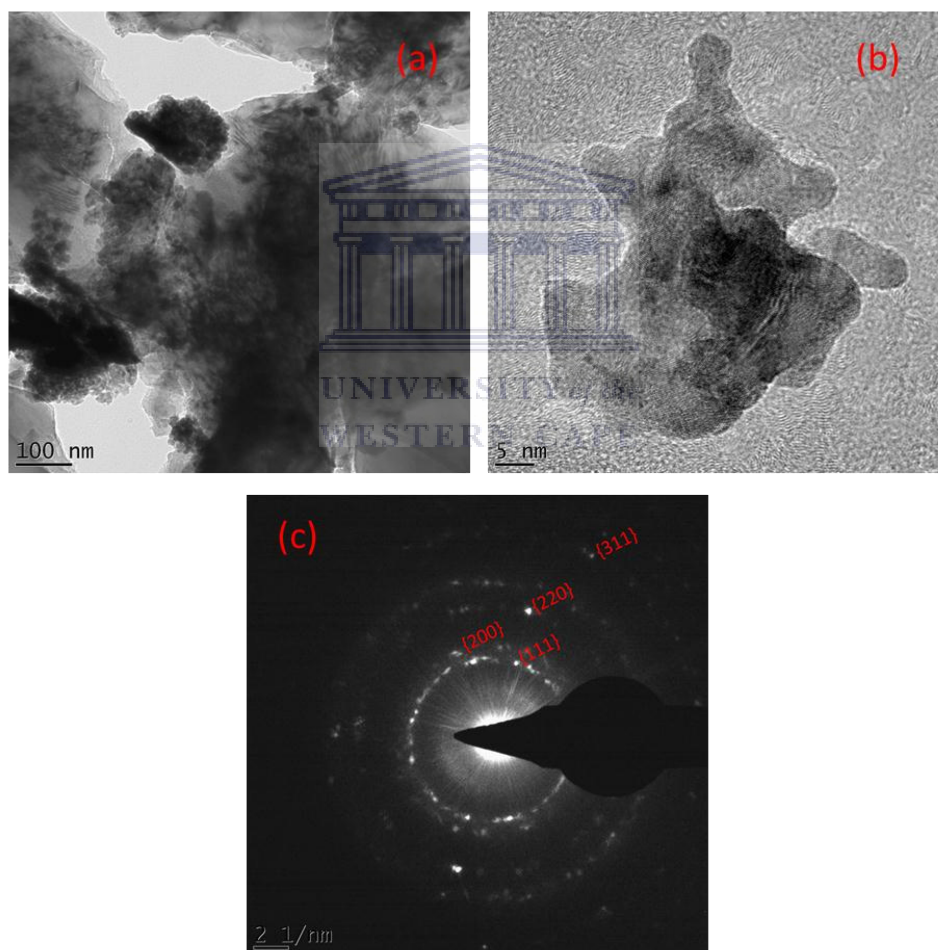

Figure 5.9: Bright field TEM images of (a) seeds on the support, (b) typical Pd clusters and (c) SAD pattern of clusters for samples M2 and M4

The micrograph on Fig 5.9 (a) shows a low magnification image of the Pd clusters (black), on pieces of the support. Fig 5.9 (b) shows a high resolution image of the Pd clusters that have formed on the support. These clusters are comprised of smaller seeds that have agglomerated as seen by the variation in lattice fringes. The SAD pattern in Fig. 5.9 (c) also confirms this as it displays the multigrain nature of the Pd clusters. The SAD pattern displayed in Fig. 5.9 (c) cannot be from the support as the SAD pattern for the support would display continuous rings as the support is polycrystalline.

Figure 5.10 shows a representative EDS spectrum for samples M2 and M4.

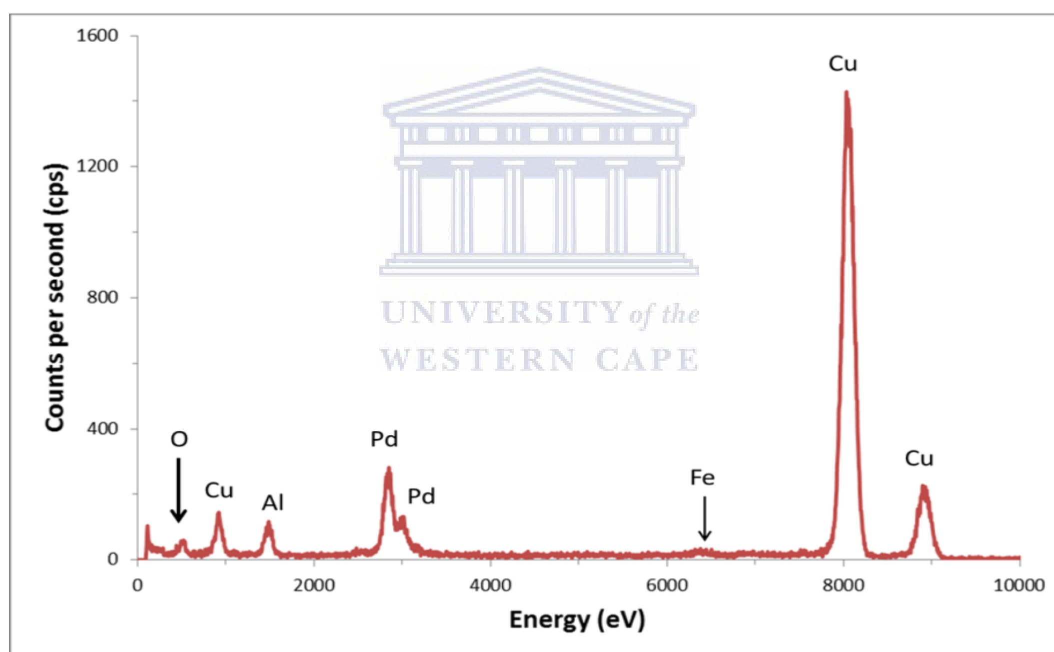

UNIVERSITY of the
WESTERN CAPE

Figure 5.10: A typical EDS spectrum for samples M2 and M4

A representative EDS spectrum for samples M2 and M4 is shown in Fig. 5.10 and confirms the same elements as found in M1 and M3 relating to the seeds, support, TEM grid as well as the traces of Fe which arise from the sample preparation method used.

5.3 Discussion of the results on seeded supports

The following assessment can be made by the analysis of the SEM and TEM images obtained from the seeded samples;

- The use of various reducing agents resulted in different seed formation. The use of dilute N_2H_4 during reduction resulted in an array of small particles, less than 15nm that completely covered the support surface as seen in Fig 5.1. The spotted face centred cubic (FCC) diffraction pattern shown in Fig. 5.7(c) shows that these particles are single crystalline in nature. In Fig 5.7(b) two different types of morphologies for the Pd is observed, namely spherical as well as the less frequent hexagonal structure. Similar morphologies for Pd seeds have also been reported previously [27].
- In Fig. 5.4 the use of H_2 as a reducing agent resulted in the formation of relatively large 3 dimensional multigrain Pd clusters. As seen in Fig 5.9 (b) the formation of these clusters is a result of particle agglomeration. Formation of these large spherical particles has also been reported previously when H_2 was used as a reducing agent [27].
- In the case of reduction by $SnCl_2$, Fig. 5.6(b), the resulting seed formation was similar to that of dilute N_2H_4. In absence of TEM images for seeds reduced with Sn^{2+}, SEM images indicate that seed sizes may be even smaller for M5 as compared to M1 and M3, as the seeds are hardly visible (compare Fig 5.1 and Fig 5.7(b) which are taken at similar magnifications).
- Tables 5.2 and table 5.4 show that supports pre-treated with APTES improved seed coverage. This highlights the ability of APTES to better attach Pd to the support surface. Without APTES heterogeneous nucleation occurs on the support surface as

UNIVERSITY of the
WESTERN CAPE

the effective surface energy is zero. Due to complete wetting during the reduction step, further deposition of the seeds on the support occur and results in an improved surface coverage as in the case of M3. The chemisorptive manner by which APTES binds Pd to the support is thus more successful in obtaining proper activation when compared to the normal physisorption which relies on the Pd atoms binding to the support via surface roughness. This result is also independent of the type of reducing agent used as both M1 and M2 exhibited this property in comparison to their counterparts M3 and M4 respectively. APTES also appears to affect the size of the seeds produced as shown by table 5.2 and Fig 5.5. Both M4 and M3 show greater seed sizes than their APTES counter parts M2 and M1 respectively.

- The elemental composition of various areas on the surface of sample M5 is shown in table 5.5. Even with the use of an acceleration step, which is supposed to remove the excess Sn, the amount of Sn present on any area of the sample ranges from 0.5-3 times the amount of Pd present in that same area. As explained previously the presence of Sn in the Pd film affects both the quality and longevity of the membrane. This is especially unfavourable for commercial use where the membrane is required to be employed for long time periods and still maintain a high selectivity.

UNIVERSITY of the
WESTERN CAPE

5.4 SEM Analysis on plated supports

SEM images of the Pd film microstructure for samples M1-M5 are shown in Fig 5.11 (a)-(e) respectively. A standard plating procedure, as outlined in section 3.4, was used for all samples. Plating times were also kept short at about 15 minutes in order to investigate the initial microstructure of the plated films.

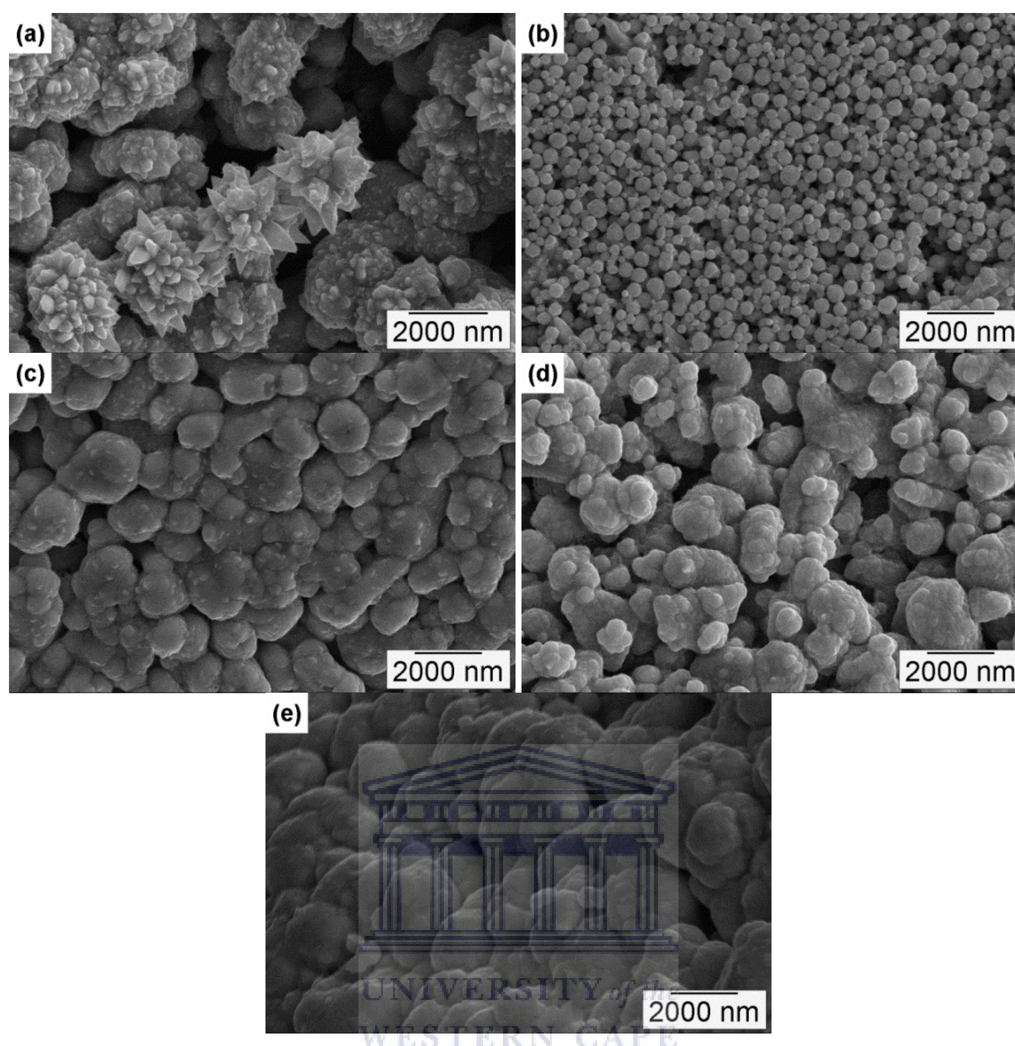

UNIVERSITY of the
WESTERN CAPE

Figure 5.11: SE images of plated samples (a) M1, (b) M2, (c) M3, (d) M4 and (e) M5

For plated sample M1 [Fig. 5.11(a)], the most notable feature is the formation of spikey particles on the upper most layer of the film. Large voids are also observed in the micrograph, as empty spaces that expose the underlying support surface in some areas. For sample M2 displayed in Fig. 5.11(b), the result is a highly porous layer, with no signs of coalescence between neighbouring particles. For sample M3 a film that consists of highly coalesced particles, with minimal voids is displayed in the micrograph Fig. 5.11(c). The film formed by sample M4 in Fig. 5.11(d) also shows areas where particle coalescence has taken place, but displays less film uniformity when compared to sample M3. For Sample M5 the

plated film consists of highly coalesced particles with minimal voids as displayed in Fig. 5.11(e). These results for sample M5 are similar to that displayed by sample M3.

Table 5.7 shows the void size ranges displayed in the films formed by samples M1-M5. Void sizes in the films formed of the various samples were measured by creating binary images of the SEM micrographs using imageJ software. This allowed for better differentiation between the Pd film particles and the voids. From the binary images void diameters were determined by the equivalent diameter approach. Table 5.8 tabulates the average Pd grain sizes of the films formed for each of the samples M1-M5, as well as the width of the size distribution of the metal grains. Grain sizes tabulated in table 5.8 were also calculated using an equivalent diameter approach.

Table 5.7: Void size ranges for samples M1-M5

Sample	Void size ranges diameter (nm)
M1	1500<
M2	NA
M3	219 – 763
M4	487 – 1213
M5	234 – 512

UNIVERSITY of the
WESTERN CAPE

Table 5.8: Characteristics of the plated film microstructure.

Sample	Average grain size (nm)	Width of size distribution (nm)
M1	1676	511
M2	-	-
M3	1191	310
M4	804	230
M5	1327	387

From table 5.7 sample M1 displays the largest void sizes of all the samples. The smallest range of void sizes is displayed by the film of sample M5. The void size ranges displayed by sample M3 are similar to that of M5. These two samples also exhibit similar grain sizes, and grain size distributions as shown in table 5.8, and also share a visual resemblance when comparing Fig. 5.11 (c) and (e).

5.5 Discussion of the results on the plated supports

It has become clear that the origin of Pd seeds have a great impact on the microstructure of the Pd deposits. Pd deposits of the APTES pre-treated samples M1 and M2 are highly porous layers of uncoalesced particles as displayed in Fig. 5.11 (a) and (b). The APTES pre-treatment does seem to promote non-continuous deposits.

In the case of sample M1 (shown in Fig. 5.11(a)) the use of APTES results in particles with an unusual spikey feature as well as large voids. The APTES pre-treated sample M2, Fig. 5.11(b), seeded with Pd using H_2 as reducing agent resulted in non-continuous uncoagulated deposits of remarkable uniform Pd spheres. This may not be very useful when dense films of Pd are required but it may find suitability for other applications, as high catalytic surface coatings. We can thus conclude that the use of APTES results in unfavourable film formation, and its use is not suitable when trying to obtain a defect free Pd film.

UNIVERSITY of the
WESTERN CAPE

Seeds prepared with N_2H_4 or H_2 as reducing agent without the use of APTES, M3 and M4 respectively, resulted in a deposition of more coalescent deposits after plating as shown in Fig. 5.11(c) and (d). The level of continuity in the deposit increases when comparing samples M4, M3 and M5. A film is observed due to coalescence of the metal grains formed.

When considering the plated samples M3, M4 and M5 it is recalled from section 5.1 that during seeding sample M5 displayed a uniform coverage of small seeds on the support. Similarly sample M3 also showed uniform coverage of the support although the seeds were found to be larger than those in sample M5. For sample M4 during seeding the support was covered in three dimensional Pd clusters, with coverage found to be less uniform when compared to samples M3 and M5. When considering table 5.7 and 5.8 the sample with the largest seeds, i.e. M4, displayed the smallest metal grain size as well as the largest sized voids. Sample M5 which has the smallest seeds displayed the largest metal grain size as well as the smallest void size range. The formation of larger metal grains brings about a reduction in the void size ranges, thus increasing the continuity displayed by the Pd film that is formed. Sample M3 which yielded seeds larger than M5 but smaller than M4, thus displays grater continuity than M4 but less than what is found in M5.

UNIVERSITY of the
WESTERN CAPE

Since the seeding conditions yielded similar results, the film formed during plating of sample M5 and M3 are similar. As explained in chapter 2 these activation methods are also more likely to form thin, i.e. less than 5µm thick, dense Pd films, because they both displayed uniform coverage of the support by seeds smaller than 10nm. After plating, samples M3 and M5 also showed similarities in their physical appearance. Both films formed by samples M3 and M5 displayed a metallic finish after plating, which was not the case for any of the other samples.

In conclusion, the seed formation method using $SnCl_2$ reduced Pd, M5, seems to give the most desired size and distribution of seeds. However, the presence of Sn needs to be avoided. Therefore, the seed formation method used to produce M3 is the recommended method for dense Pd membrane fabrication.

5.6 Permeance results and discussion on electroless plated samples

Based on the findings in section 5.5, seeding method M3 was used to seed two different supports. Support type 1 was the Al_2O_3 tubular supports that were used throughout the seeding experiments. Support type 2 was an in house synthesized ZrO_2 support, prepared by a fellow student whose MSc was related to the synthesis of ZrO_2 hollow fibres [28]. In comparison to the commercially obtained Al_2O_3 supports, the ZrO_2 supports exhibited a smoother surface as well as smaller pore sizes. These are favourable support characteristics when trying to achieve dense thin film Pd membranes.

All seeded samples were subjected to an identical plating procedure. In order to determine to what extend the seeding method influences the ability to produce a continuous film, the plated samples were subjected to a permeance measurement using N_2 at different temperatures, 25^oC and 320^oC, and H_2 at 320^oC. The temperature of 320^oC was the maximum allowable temperature for the gasket material.

UNIVERSITY of the
WESTERN CAPE

As a sealant, Red RTV Gasket Maker obtained from a local hardware store was used by applying it to the ends of the plated supports. One end was secured to the module at the feed side with the other end sealed off as shown in Fig. 4.6. The use of this sealant was deemed possible as it allowed permeance testing to be conducted above the critical temperature of 298° in order to avoid H_2 embrittlement in the membranes. All other relevant sample details are given in Table 5.9 below. As indicated, different levels of Vacuum suction was applied during the plating procedures. Before any ZrO_2 or Al_2O_3 supported membranes were tested, a support of each type, completely covered with sealant was tested at the various conditions. The results showed no permeance for both H_2 and N_2 at both room temperature and at 320^oC. This confirmed that a gas tight seal was

obtained, and also confirmed the suitability of the sealant employed during the testing of the various membranes. Table 5.9 shows the characteristics of all samples that were prepared for permeance testing.

Table 5.9: Characteristics of the ELP membranes subjected to permeance testing

Sample	Support	Seeding Method	Plating Time (min)	Vacuum Strength (bar)
A0	Al_2O_3	none	none	NA
A1	Al_2O_3	#3	60	NA
A2	Al_2O_3	#3	60	0.8
A3	Al_2O_3	#3	60	0.2
Z0	ZrO_2	none	none	NA
Z1	ZrO_2	#3	60	0.8
Z2	ZrO_2	#3	60	0.6
Z3	ZrO_2	#3	60	0.4
Z4	ZrO_2	#3	60	0.2

UNIVERSITY of the
WESTERN CAPE

Fig. 5.12 shows a plot of the permeance results obtained for samples A0-A3 using N_2 gas at room temperature. Sample A0 was the blank, i.e. unseeded and unplated support, and was used a reference.

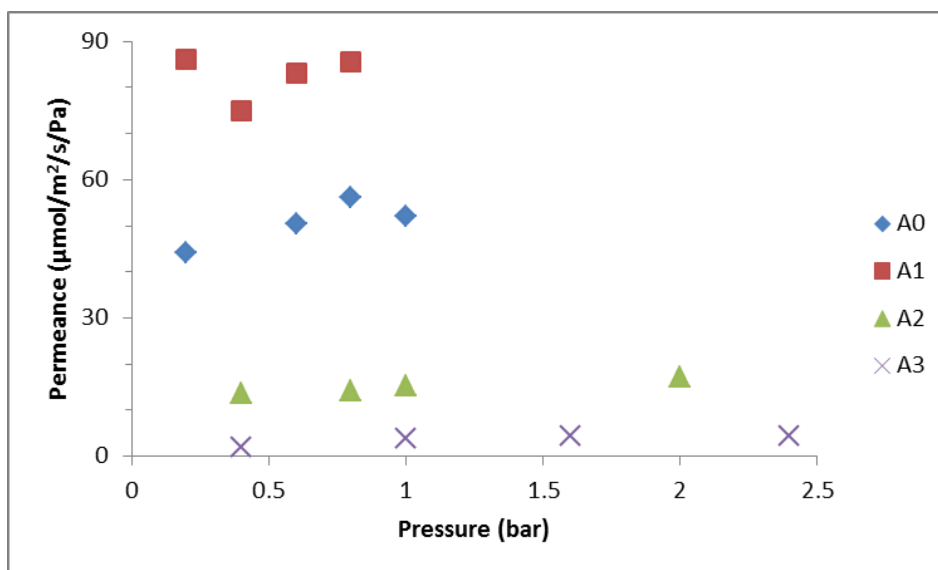

Figure 5.12: Permeance results for samples A0-A3 using nitrogen gas at room temperature

In Fig. 5.12 sample A1 showed the greatest permeance, nearly double that of A0 which is the blank support when tested at room temperature using N_2 gas. A low permeance of about 15 µmol.m^{-2}.s^{-1}.Pa^{-1} was obtained for sample A2, while sample A3 showed even lower permeance at around 2 µmol.m^{-2}.s^{-1}.Pa^{-1}.

UNIVERSITY of the
WESTERN CAPE

Low temperature N_2 permeance testing is an ideal way to characterize membrane performance [29]. All of the Al_2O_3 supported membranes exhibited some N_2 permeance when tested at room temperature. The permeance displayed A1 in Fig. 5.12 indicates some viscous flow. Viscous flow or Poiseuille flow is characterised by elastic collisions between molecules which occur more frequently than molecule-wall collisions [29]. In this regime a membrane displays zero selectivity. With the exception of A1 the results indicate that the use of vacuum during the plating procedure does have an impact on the formation of a dense pd film. The lower N_2 permeance exhibited by A3 in comparison to samples A0 and A2 shows that at higher vacuum, more of the support pores are filled by the Pd, and limits the permeation of the N_2 through the sample.

Fig. 5.13 displays a plot of the permeance results obtained for samples A2 and A3 at 320°C for both H_2 and N_2.

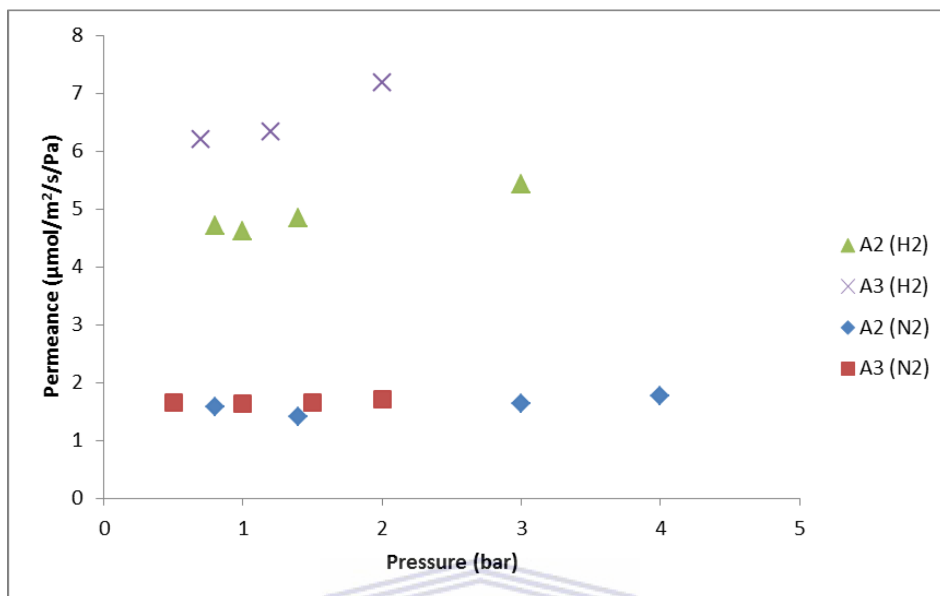

Figure 5.43: Permeance results for samples A2 and A3 at 320°C

For both A2 and A3 a decrease in the N_2 permeance at higher temperature is observed. This is expected as the increase in temperature results in a lower concentration of gas molecules at the same pressure. The result is a decrease in permeance, as diffusion in the membrane is driven by the concentration gradient of the gas.

UNIVERSITY of the
WESTERN CAPE

The selectivity (α) of the samples shown in table 5.10 were calculated using the ratio of average H_2 and N_2 permeance of each sample at 320°C.

Table 5.10: Selectivity of samples A2 and A3

Sample	***Selectivity ($\alpha_{H2/N2}$)***
A2	*3.07*
A3	*3.34*

Selectivity of both samples A2 and A3 are similar and suggest a Knudsen based diffusion mechanism. The selectivity of A3 is somewhat closer to theoretical value of Knudsen based selectivity, which is calculated by the inverse ratio of the square-roots of the molecular weights (M) of the gasses ($\alpha_{Knudsen} = \sqrt{\frac{M_{N_2}}{M_{H_2}}} = 3.74$).

These results confirm that none of the Al_2O_3 supported samples fabricated were dense. Based on the SEM results obtained in section 5.4, this is no surprise as the Pd deposits are not entirely coalesced. The application of a vacuum during plating did unfortunately not secure the formation of a dense layer. As noted in literature, a dense layer of Pd is difficult to achieve on a support as rough as the Al_2O_3 used in this part of the study.

Table 5.11 shows the results obtained for samples ZrO2 supported Pd (Z0-4). Sample Z0 was the blank, i.e. unseeded and unplated, and was used a reference.

UNIVERSITY of the
WESTERN CAPE

Table 5.11: Permeance results for ZrO_2 supported membranes Z0 to Z4

Sample	Pressure (bar)	Tempreture (^oC)	Gas	Permence ($\mu mol.m^{-2}.s^{-1}. Pa^{-1}$)	Selectiviy H_2:N_2
Z0	1	25	N_2	7.53	0
Z0	2	25	N_2	7.8	
Z0	3	25	N_2	8.66	
Z0	4	25	N_2	9.51	
Z0	4	320	N_2	0	
Z0	4	320	H_2	0	
Z1	4	25	N_2	0	0
Z1	4	320	N_2	0	
Z1	4	320	H_2	0	
Z2	4	25	N_2	0	infinite
Z2	4	320	N_2	0	
Z2	4	320	H_2	0.062	
Z3	4	25	N_2	0	2.71
Z3	3	320	N_2	0.061	
Z3	4	320	N_2	0.08	
Z3	2	320	H_2	0.16	
Z3	3	320	H_2	0.18	
Z3	4	320	H_2	0.24	
Z4	4	25	N_2	0	0
Z4	4	320	N_2	0	
Z4	4	320	H_2	0	

UNIVERSITY of the
WESTERN CAPE

Permeance through the blank, Z0, at room temperature using N_2 was obtained, but no signs of permeation were shown when tested at 320^oC for either H_2 or N_2. The same permeance was also obtained after cooling the sample down to room temperature again. In other words, the closure of the permeating path at higher temperatures seemed to be reversible which is a highly remarkable result. These permeance results came after the other samples were already plated. It became apparent that this particular batch of ZrO_2 hollow fibres were calcined at 1550^oC degrees, 100^oC higher than the samples prepared by B.M

Tshamano [28]. This had resulted in the production of a dense support structure. There is however, little value in coating supports with Pd that are already dense at higher temperatures. Unfortunately, no other porous ZrO_2 samples were available for plating. Analysis of the Z1-Z4 does however show some interesting results.

- Samples Z1 and Z4 exhibited no permeance when testing the membranes with either H_2 or N_2, at both high and low temperatures. It is possible that the Pd films formed on top of these supports were dense as they also showed zero permeance during low temperature N_2 testing.
- Sample Z3 only exhibited permeance during high temperature N_2 and H_2 testing. This suggests that the Pd deposits covered the support well enough to prevent any N_2 to permeate during testing at room tempreture. The permeance observed at high temperature of both N_2 and H_2, suggests that a defect or crack had formed during the heating or testing procedures.

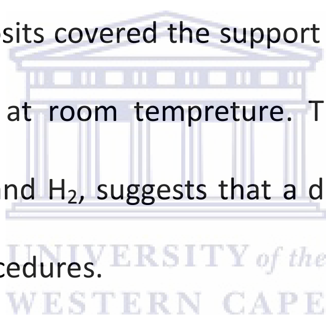
UNIVERSITY of the
WESTERN CAPE

- Sample Z2 shows H_2 permeance at elevated temperature but no N_2 permeance. It is suggested that this particular sample contains defects in the dense ZrO_2 support structure (otherwise the permeation value for H_2 would also be zero) and during the plating procedure, these defects had been covered with a dense film of Pd, thus creating a permeation path for the H_2. The resulting membrane shows infinite selectivity. By lack of the availability of other ZrO_2 support samples, this results is promising for future membrane fabrication when employing seeding method M3.

Chapter 6: Conclusion and Recommendations

6.1 Conclusion

SEM results showed that all the seeding methods, M1-M4, yielded large amounts of Pd seeds, with good distribution on the support. Samples that were pre-treated with APTES showed higher levels of uniformity than those that weren't. However in respect to initial film microstructure after plating the APTES activated samples produced films with lower levels of continuity. APTES also showed signs of possibly hindering seed growth and thus negatively affected the plating procedure by producing Pd films of poor quality when compared to the methods which did not make use of APTES. Sample M5 was fabricated to act as a standard to which to compare the samples M1 – M4, as the seeding method employed by M5 is known to produce high quality dense Pd membranes. However the use of this conventional method, in sample M5, is unfavourable as it degrades the Pd film over long periods due to Sn contamination. The presence of Sn on the surface of seeded samples was confirmed even when an acceleration step was employed in the seeding procedure.

UNIVERSITY of the
WESTERN CAPE

Of all the seeding methods employed, sample M3 showed great similarities to that of M5 i.e. Small seeds, around 10nm, with uniform coverage, as well as similar film microstructure. Not only is this method well-suited for a dense Pd film, but it is also simplistic and can easily be employed in industry.

As the seeding method for sample M3 was the method of preference, the goal was to use it in membrane fabrication to acquire a dense membrane, and thus confirm the analysis. Initially, Al_2O_3 tubes were seeded using method M3 and plated. Vacuum was applied during the plating procedure in an attempt to produce a defect free film. The permeance tests on

these samples showed selectivity close to Knudsen diffusion, a sign that the Pd deposits did not form a dense layer. The Al_2O_3 support was then replaced by ZrO_2 hollow fibres with a much smoother surface.

Unfortunately the available fibres were produced in a newly made induction furnace and sintered at a higher temperature than previous batches. The higher sintering temperature has resulted in the production of fibres that appeared dense when tested above 300^oC. Most of the ZrO_2 supported samples appeared to be dense as they exhibited zero N_2 permeance during low temperature testing. Only one sample appeared to show high selectivity towards H_2. It is possible that this particular sample exhibited some defects in the ZrO_2 structure. A dense Pd film plated on top of this defect caused the membrane to show infinite selectivity towards H_2. The fabrication of these types of samples indicates that dense Pd membrane fabrication can be achieved when using the M3 seeding method.

UNIVERSITY of the
WESTERN CAPE

6.2 Suggestions

It is suggested that work be continued on membrane fabrication using the seeding method recommended in this study, in order to reproducibly obtain membranes of high quality and selectivity. Also as seen in SEM results, a further study can be done to understand the mechanisms and kinetics behind the formation of the different types of seeds when using different reducing agents. The densification of the ZrO_2 supports at high temperatures should also be investigated.

References:

[1] Yun, S., Oyama, T., 2011, Correlations in palladium membranes for hydrogen separation: A review, Journal of membrane science, (375) pg. 28-45

[2] Holladay, J.D., Hu, J., King, D.L., Wang, Y., 2009, An overview of hydrogen production technologies, Catalysis Today, (139) pg. 244-260

[3] Li, H., Goldbach, A., Li, W., Xu, H., 2008, On CH_4 decomposition during separation from H2 mixtures with thin Pd membranes, Journal of membrane science, (324) pg. 95-101

[4] Jung, S.H., Kusakabe, K., Morooka, S., Kim, S.D., 2000, Effects of co-existing hydrocarbons on hydrogen permeation through a palladium membrane, Journal of membrane science, (170) pg. 53-60

[5] A., Basile, F., Gallucci, S. Tosti, 2008, Synthesis, characterisation and applications of palladium membranes, Membrane science and technology, (13) pg. 255-317

[6] Paglieri, S.N., Way, J.D., 2002, Innovations in palladium membrane research, Separation and Purification Reviews, (31:1) pg. 1-169

[7] Cheng, Y.S., Yeung, K.L., 2001, Effects of electroless plating chemistry on the synthesis of palladium membranes, Journal of Membrane Science, (182) pg. 195-203

[8] Huang, Y., Dittmeyer, R., 2007, Preperation of thin palladium membranes on a porous support with rough surface, Journal of Membrane Science, (302) pg.160-170

UNIVERSITY of the
WESTERN CAPE

[9] Suleimanova, R.S., Mukasyan, A.S., Varma A., 2000, Effects of Osmosis on microstructure of Pd-composite membranes synthesized by electroless plating technique, Journal of membrane science, (166) pg.249-257

[10] Williams, M., Bladdergroen, B., 2008, Surface funtionalisation of porous ZrO2-TiO2 membranes using γ-aminopropyltriethoxyssilane in palladium electroless deposition, Applied Surface Science, (254) pg. 3211-3219

[11] Tong. J., Su, L., Haraya, K., Suda, H., 2008, Thin Pd membrane on α-Al2O3 hollow fibre substrate without any interlayer by electroless plating combined with embedding Pd catalyst in polymer template, Journal of membrane science, (310) pg. 93-101

[12] Okazaki, J., Ikeda, T., David, A., Tanaka, P., Tanco, M.A.L, Wakui, Y., Sato, K., Mizukami, F., Suzuki, T.M, 2009, Importance of the support material in thin palladium composite membranes for steady hydrogen permeation at elevated temperatures ,www.rsc.org/pccp, 15 November 2013

UNIVERSITY of the
WESTERN CAPE

[13] Maneerung, T., Hidajat, K., Kawi, S., 2014, Ultra-thin(<1 μm) internally-coated Pd–Ag alloy hollow fibre membrane with superior thermal stability and durability for high temperature H_2 separation, Journal of membrane science, (452) pg. 127-142

[14] Jun, C. S., Lee, K. H., 2000, Palladium and Palladium alloy composite membranes prepared by metal-organic chemical vapour deposition (cold-wall), Journal of membrane science, (176) pg. 121-130

[15] Itoh, N., Akiha, T., Sato, T., 2005, Preparation of thin Palladium composite membrane tube by a CVD technique and its hydrogen permselectivity, Catalysis Today, (104) pg. 231-237

[16] Ryi, S. K., Park, J. S., Kim, S. H., Cho, S. H., Kim, D. W., Um, K. Y., 2006,Characterisation of Pd-Cu-Ni ternary alloy membrane prepared by magnetron sputtering and Cu reflow on porous nickel support for hydrogen separation, Seperation and Purification Technology, (50) pg. 82-91

[17] Chen, S. C., Tu, G. C., Hung, C. C. Y., Huang, C. A., Rei, M. H., 2008, Preperation of Palladium membrane by electroplating on AISI 316L porous stainless steel supports and its use for methanol steam reformer, Journal of membrane science, (314) pg. 5-14

[18] Kroschwitz, J.I., Howe-Grant, M., 2001, Electroless Plating in Kirk-Othmer encyclopedia fourth edition, Wiley and Sons, New York

[19] Hornyak, G.L., Dutta, J., Tibbals, H.F., Rao, A.K., 2010, Introduction to Nanoscience, CRC Press, Taylor and Francis,London, New York

[20] Zhao, H.B., Pflanz, K., Gu, J.H., Li, A.W., Stroh, N., Brunner, H., Xiong, G.X., 1998, Peperation of palladium composite membranes by modified electroless plating procedure, Journal of membrane science, (142) pg. 147-157

[21] Suleimanova, R.S., Mukasyan, A.S., Varma, A., 1999, Study of the structure formation during electroless plating of thin metal-composite membranes, Chemical Engineering Science, (54) pg. 3369-3377

[22] Ayturk, M. E., Ma, Y. H., 2009, Electroless Pd and Ag deposition kinetics of the composite Pd and Pd/Ag membranes synthesised from agitated plating baths, Journal of membrane science, (330) pg. 233-245

UNIVERSITY of the
WESTERN CAPE

[23] Paglieri, S.N., Foo, K.Y., Way, J.D., Collins, J.P., Harper-Nixon, D.L.,1999, A new preparation technique for Pd/alumina membranes with enhanced high-temperature stability, Ind. Eng. Chem. Res., (38) pg. 1925-1936

[24] Dressick, W.J., Kondracki, L.M., Chen, M., Brandow, S.L., Matijevic, E., Calvert, J.M., 1996, Characterisation of a Colloidal Pd(II)-based catalyst dispersion for Electroless Metal Deposition , Colloids and Surfaces A: Physiochemical and Engineering Aspects, (108) pg. 101-111

[25] Goodhew, P.J., Humphreys, J., Beanland, R., 2001, Electron Microscopy and Analysis third edition, Taylor and Francis, New York

[26] Postek, M.T., Howard, K.S., Johnson, A.H., McMichael, K.L, 2001, Scanning Electron Microscopy, Ladd Research Institute, Vermont

[27]Choo, H., He, B., Liew, K.Y., Liu, H., Li, J., 2006, Morphology and control of Pd nanoparticles, Journal of molecular catalysis, (244) pg. 217-228

[28] Tshamano, B.M, 2013, Synthesis & characterization of yttria-stabilised zirconia (YSZ) hollow fibre support for Pd based membrane, MSc thesis, University of the Western Cape

[29] Pabby, A.K., Rizvi, S.S.H., Sastre, A.M., 2008, Handbook of Membrane Separations Chemical, Pharmaceutical, Food, and Biotechnological Applications, CRC Press, Taylor and Francis,NewYork

UNIVERSITY of the
WESTERN CAPE

UNIVERSITY of the
WESTERN CAPE